

## REVIEW

[View Article Online](#)  
[View Journal](#) | [View Issue](#)Cite this: *Chem. Sci.*, 2024, 15, 5897

## Single-atom and cluster catalysts for thermocatalytic ammonia synthesis at mild conditions

Xuanbei Peng,<sup>†ab</sup> Mingyuan Zhang,<sup>†a</sup> Tianhua Zhang,<sup>†a</sup> Yanliang Zhou,<sup>\*ab</sup> Jun Ni,<sup>a</sup> Xiuyun Wang<sup>ID</sup><sup>\*ab</sup> and Lilong Jiang<sup>ID</sup><sup>\*ab</sup>

Ammonia (NH<sub>3</sub>) is closely related to the fields of food and energy that humans depend on. The exploitation of advanced catalysts for NH<sub>3</sub> synthesis has been a research hotspot for more than one hundred years. Previous studies have shown that the Ru B<sub>5</sub> sites (step sites on the Ru (0001) surface uniquely arranged with five Ru atoms) and Fe C<sub>7</sub> sites (iron atoms with seven nearest neighbors) over nanoparticle catalysts are highly reactive for N<sub>2</sub>-to-NH<sub>3</sub> conversion. In recent years, single-atom and cluster catalysts, where the B<sub>5</sub> sites and C<sub>7</sub> sites are absent, have emerged as promising catalysts for efficient NH<sub>3</sub> synthesis. In this review, we focus on the recent advances in single-atom and cluster catalysts, including single-atom catalysts (SACs), single-cluster catalysts (SCCs), and bimetallic-cluster catalysts (BCCs), for thermocatalytic NH<sub>3</sub> synthesis at mild conditions. In addition, we discussed and summarized the unique structural properties and reaction performance as well as reaction mechanisms over single-atom and cluster catalysts in comparison with traditional nanoparticle catalysts. Finally, the challenges and prospects in the rational design of efficient single-atom and cluster catalysts for NH<sub>3</sub> synthesis were provided.

Received 30th December 2023

Accepted 7th March 2024

DOI: 10.1039/d3sc06998b

[rsc.li/chemical-science](https://rsc.li/chemical-science)

## 1. Introduction

The excessive consumption of conventional fossil fuels in the modern industrial world has led to the increasing pressure of energy crisis and environmental pollution on human society.<sup>1</sup> To achieve the goal of zero carbon emissions in 2060, there is an urgent need to develop and utilize renewable and environmentally friendly energy sources so as to move towards a low-carbon society and economy. However, sustainable and renewable energy face a compatibility issue with the current large-scale and established energy infrastructure because of their intrinsic intermittence and fluctuation. The application of energy storage carrier is an efficient route to solve the utilization of renewable energy. It is general knowledge that hydrogen serves as a clean energy. Recently, with the green generation of electricity using renewable sources (such as hydro, wind, solar and tidal), it becomes economically acceptable to use the H<sub>2</sub> produced by water electrolysis. However, high pressure transportation (~20 MPa) currently hinders its large-scale application.<sup>2</sup> Therefore, it is important to develop hydrogen production, storage and transportation systems that allow hydrogen to be distributed and utilized in a safe manner.<sup>3</sup>

Ammonia (NH<sub>3</sub>) is an important chemical product with a wide range of applications in modern society, such as the production of fertilizers, pharmaceuticals, explosives, and other nitrogen-containing compounds.<sup>4–6</sup> In addition, NH<sub>3</sub> is also a promising carbon-free energy storage carrier for storing intermittent renewable energy sources.<sup>7,8</sup> Compared to liquid hydrogen and other organic liquid hydrogen energy carriers (such as toluene and cyclohexane),<sup>3</sup> NH<sub>3</sub> is preferred as an energy carrier due to its high energy density (4.32 kW h L<sup>−1</sup>), high gravimetric (17.6 wt%) and volumetric (121 kg m<sup>−3</sup>) hydrogen densities, and ease of liquefaction under mild conditions.<sup>9–12</sup> Moreover, the storage and transportation systems of liquid NH<sub>3</sub> are mature and safe.<sup>9</sup> Currently, the industrial production of NH<sub>3</sub> is mainly through the Haber–Bosch (HB) process using Fe-based catalysts at high temperatures (490–510 °C) and high pressures (15–30 MPa).<sup>13,14</sup> To meet the global demand for NH<sub>3</sub>, approximately 200 million tons of NH<sub>3</sub> are produced annually using the HB process, which consumes about 1–2% of the global annual energy supply and also results in significant carbon dioxide emissions.<sup>5,15–17</sup> With the maturity of water electrolysis technology driven by renewable electric power, the carbon emission problem in NH<sub>3</sub> synthesis will be solved properly by coupling water electrolysis for H<sub>2</sub> production technology with the electrolysis-driven HB (eHB) process.<sup>18–20</sup> The present bottleneck is that NH<sub>3</sub> cannot be synthesized under mild conditions, resulting in mismatch with the pressure of the electrolysis system employed for H<sub>2</sub> production (<5 MPa, mostly in the range of 1.0–3.2 MPa).

<sup>a</sup>National Engineering Research Center of Chemical Fertilizer Catalyst, Fuzhou University, Fuzhou, Fujian, 350002, China. E-mail: zhouyl@fzu.edu.cn; xywangfzu@163.com; jll@fzu.edu.cn

<sup>b</sup>Qingyuan Innovat Lab, Quanzhou, Fujian, 362801, China

<sup>†</sup> These authors contributed equally to this work.

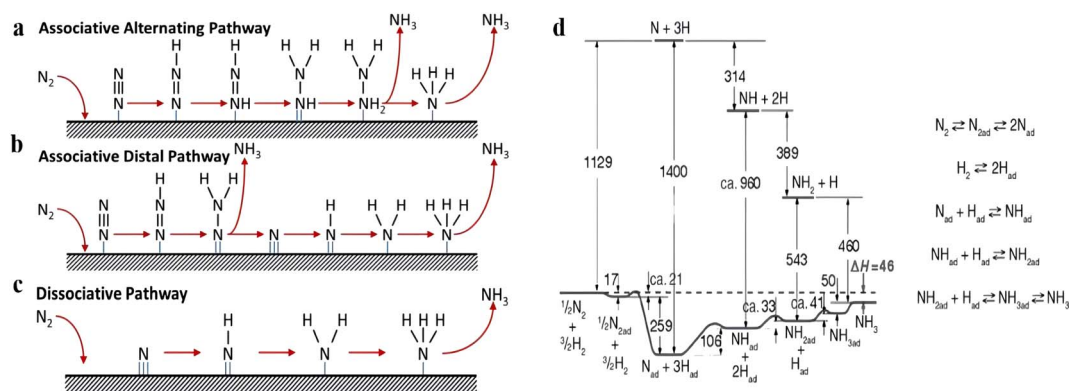
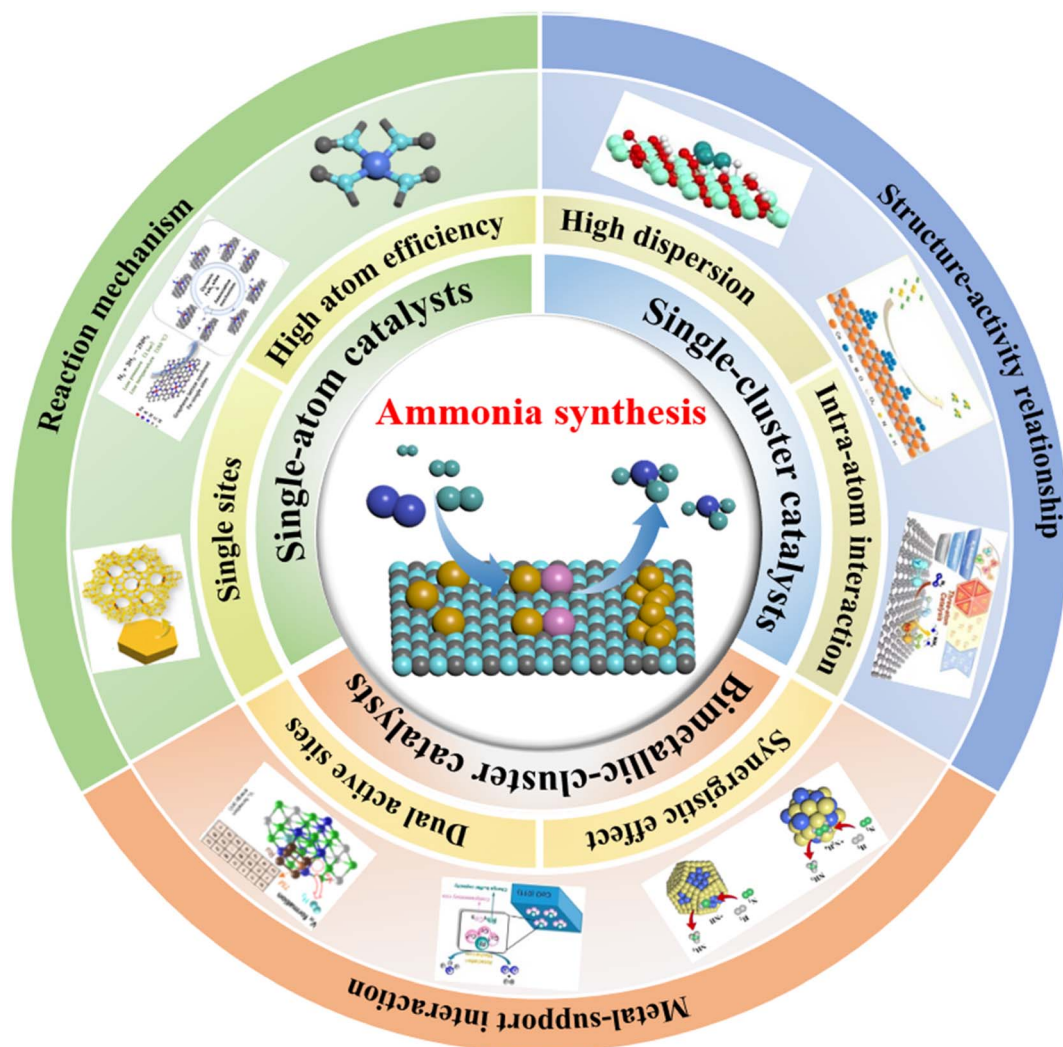


Fig. 1 (a) Associative alternating pathway, (b) associative distal pathway, and (c) dissociative pathway for  $\text{NH}_3$  synthesis on heterogeneous catalysts.<sup>21</sup> (d) Mechanism and potential energy diagram of  $\text{NH}_3$  synthesis on the iron surface.<sup>22</sup>

Accordingly, the design and development of efficient  $\text{NH}_3$  synthesis catalysts under mild conditions are keenly needed.

The main bottleneck for the synthesis of  $\text{NH}_3$  is the activation of the inert  $\text{N}_2$ , primarily due to its high  $\text{N}\equiv\text{N}$  triple bond energy

(941  $\text{kJ mol}^{-1}$ ), lack of a permanent dipole, a large HOMO–LOMO gap (10.8 eV) and a high ionization energy (15.58 eV),<sup>23,24</sup> making it difficult to activate under mild conditions. At present, the activation route of  $\text{N}_2$  has been widely studied, which involves



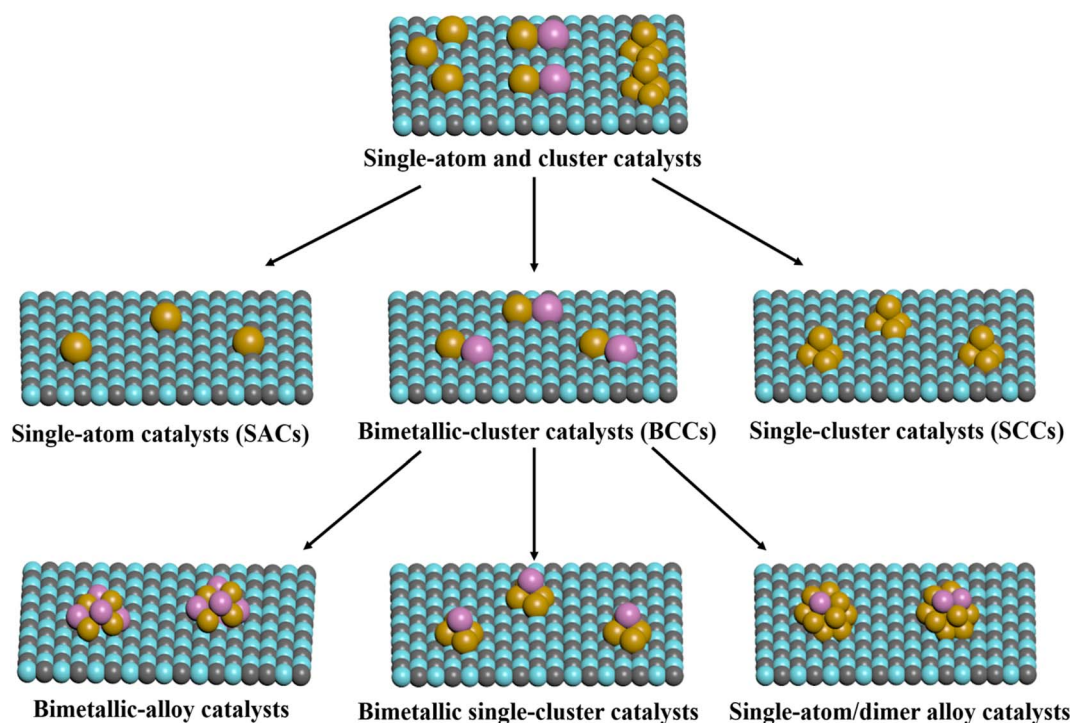
Scheme 1 Schematic for single-atom and cluster catalysts for thermocatalytic  $\text{NH}_3$  synthesis.



either the associative or dissociative route. In both photocatalytic and electrocatalytic synthesis of  $\text{NH}_3$ , the mild reaction conditions cannot realize the direct dissociation of the  $\text{N}\equiv\text{N}$  triple bond while enabling the hydrogenation of  $\text{N}_2$  *via* an associative mechanism with the assistance of an external field (Fig. 1a and b).<sup>25–27</sup> For alternate hydrogenation, the two N atoms are hydrogenated by protons to form  $^*\text{NH}-\text{NH}$  and  $^*\text{NH}_2-\text{NH}_2$  species, whereas for distal hydrogenation, protons are bonded to one N atom to form the  $^*\text{N}-\text{NH}_2$  and  $^*\text{N}-\text{NH}_3$  species. Comparatively, due to the existence of certain temperature and pressure in the thermocatalytic  $\text{NH}_3$  synthesis,  $\text{N}_2$  is more likely to form  $\text{NH}_3$  *via* the dissociative mechanism, whereby the adsorbed  $\text{N}_2$  dissociates directly into the adsorbed N atoms ( $2\text{N}$ ), followed by stepwise hydrogenation to form  $\text{NH}_3$  (Fig. 1c). As early as 1934, Emmett and Brunauer speculated that the formation rate of  $\text{NH}_3$  should be approximately equal to the dissociation rate of  $\text{N}_2$  on the surface of the iron-based catalysts.<sup>28</sup> Subsequently, Ertl and his colleagues further confirmed this viewpoint through a series of surface characterization techniques on Fe-based catalysts, and they revealed the process of  $\text{NH}_3$  synthesis *via* a dissociative mechanism (Fig. 1d).<sup>22,29,30</sup> Concurrently, the dissociative adsorption of  $\text{N}_2$  is generally considered as the rate-determining step (RDS) for  $\text{NH}_3$  synthesis, which is closely related to unique active sites on the transition metal surface, such as the  $\text{C}_7$  sites of Fe.<sup>31,32</sup> The so-called  $\text{C}_7$  active sites mean seven adjacent Fe atoms on the surface of an Fe single crystal.<sup>33,34</sup> Somorjai and Strongin *et al.* studied the high-pressure  $\text{NH}_3$  synthesis on different crystal faces of Fe single crystal and found that the  $\text{NH}_3$  synthesis activity presented in the following order:  $\text{Fe (111)} > \text{Fe (211)} > \text{Fe (100)} > \text{Fe (210)} > \text{Fe (110)}$ .<sup>31,34–37</sup> The catalytic activity of Fe (111)

and (100) surfaces was *ca.* 418 and 25-fold higher than that of tightly packed Fe (110) surfaces, respectively, indicating that the  $\text{NH}_3$  synthesis over Fe catalysts is a structure-sensitive reaction. The high activity of  $\text{NH}_3$  synthesis at Fe (111) was mainly attributed to the presence of a large number of  $\text{C}_7$  active sites, which facilitated the significant weakening of the  $\pi$  bond in  $\text{N}\equiv\text{N}$  and promoted its dissociation.<sup>31</sup> The dissociative mechanism on the Fe (111) surface was also further verified by Nørskov *et al.* using density functional theory (DFT) calculations.<sup>38</sup>

Compared with Fe-based catalysts, the  $\text{NH}_3$  synthesis over Ru is considered to be more structurally sensitive through DFT calculations and extensive studies on Ru single crystals.<sup>39–41</sup> Moreover,  $\text{N}_2$  dissociation on Ru (0001) surface was considered to be entirely dominated by the  $\text{B}_5$  sites,<sup>39,40</sup> which exposed a three-fold hollow site with a bridge site in close proximity to assure two nitrogen atoms of  $\text{N}_2$  not bonding to the same Ru atom. The concentration of the  $\text{B}_5$  sites strongly depends on the size and shape of Ru nanoparticles (Ru NPs), with the highest concentration of  $\text{B}_5$  active sites in 1.8–2.5 nm Ru NPs, whereas almost no  $\text{B}_5$  active sites exist when the particle size of Ru NPs is less than 1.8 nm.<sup>33,42,43</sup> In the past few decades, numerous efforts have been made to develop various high-performance transition metal catalysts to lower the dissociation energy of  $\text{N}_2$ , but only a few novel catalysts have been able to shift the bottleneck from slow  $\text{N}_2$  dissociation to the formation of  $\text{N}-\text{H}_x$  ( $x = 1-3$ ).<sup>44–46</sup> In recent years, theoretical and experimental studies have demonstrated that in thermocatalytic  $\text{NH}_3$  synthesis, when the particle size of metal nanoparticles is reduced to the sub-nanometer clusters, atomic clusters or even single atom level, in which effective sites for  $\text{N}_2$  dissociation cannot be formed;  $\text{N}_2$  is



Scheme 2 Schematic diagram of classification over single-atom and cluster catalysts.





inclined to be activated *via* an associative mechanism for  $\text{NH}_3$  synthesis.<sup>47–49</sup> It has been shown that controlling active metal in the form of subnano clusters or single atoms is an efficient method to improve their catalytic activity and utilization.<sup>49–51</sup> Therefore, transition metal catalysts at the nanoscale, sub-nanoscale, especially at the atomic level, have received widespread attention in the field of  $\text{NH}_3$  synthesis in recent years.

In this review, the recent progress in single-atom and cluster catalysts, including SACs, SCCs, and BCCs, for thermocatalytic  $\text{NH}_3$  synthesis is presented for both the theoretical development and experimental practice (Schemes 1 and 2). The unique properties and reaction mechanisms over single-atom and cluster catalysts compared with traditional nanoparticle catalysts are discussed and summarized. In addition, we also discuss the current challenges and future prospects of the design of single-atom and cluster catalysts for  $\text{NH}_3$  synthesis under mild conditions. The purpose of this review is to deepen the fundamental understanding and give guidance for the rational design of advanced catalysts for  $\text{NH}_3$  synthesis.

## 2. SACs for $\text{NH}_3$ synthesis

In recent years, SACs have garnered widespread attention in the field of heterogeneous catalysis for their maximum atom efficiency and excellent catalytic performance, mainly due to the significant advantages of SACs in terms of activity, selectivity, and tunable interactions between metal atoms and supports.<sup>52–54</sup> Currently, there are various synthesis methods for SACs, such as high-temperature pyrolysis,<sup>55</sup> co-precipitation,<sup>56</sup> one-pot synthesis,<sup>57</sup> and atomic layer deposition (ALD).<sup>58</sup>

However, isolated metal atoms with high surface free energy are prone to migrate and aggregate under reaction conditions. Therefore, various supports including carbon materials, nitrogen-doped carbon-based materials, metal oxides, and zeolites are typically employed in the preparation process to disperse and stabilize metal atoms.<sup>59–61</sup> Besides, according to the property of active metal in SACs for  $\text{NH}_3$  synthesis, it can be simply classified as noble metal SACs and non-noble metal SACs.

### 2.1 Noble metal SACs

Noble metals, which are active for  $\text{NH}_3$  synthesis, are mainly represented by Os and Ru. Therein, the research and application of Os is limited because of its scarcity, while Ru-based catalysts are regarded as the second-generation catalysts for  $\text{NH}_3$  synthesis. Due to the high cost of the noble metal Ru, developing Ru SACs can maximize its atomic efficiency while providing well-defined single-atom sites for mechanism study.<sup>62</sup> Qiu *et al.* prepared pure siliceous zeolite-supported Ru single-atom catalyst (Ru SAs/S-1) using hydrothermal and vacuum decomposition methods (Fig. 2a).<sup>63</sup> At 523–648 K and 0.1 MPa, the  $\text{NH}_3$  synthesis rate of Ru SAs/S-1 was higher than that of the traditional Cs–Ru/MgO catalyst with similar Ru content (Fig. 2b), indicating that the single Ru active site exhibited excellent catalytic performance, which was associated with its distinct  $\text{N}_2$  activation pathway. The  $\text{N}_2$  reaction order of Ru SAs/S-1 was determined to be 0.15, which was much lower than that of traditional Ru-based catalysts (close to unity), indicating that the dissociation of  $\text{N}_2$  was no longer the rate-determining step.<sup>64</sup> Moreover, the  $\text{H}_2$  reaction order over Ru SAs/S-1 is a positive

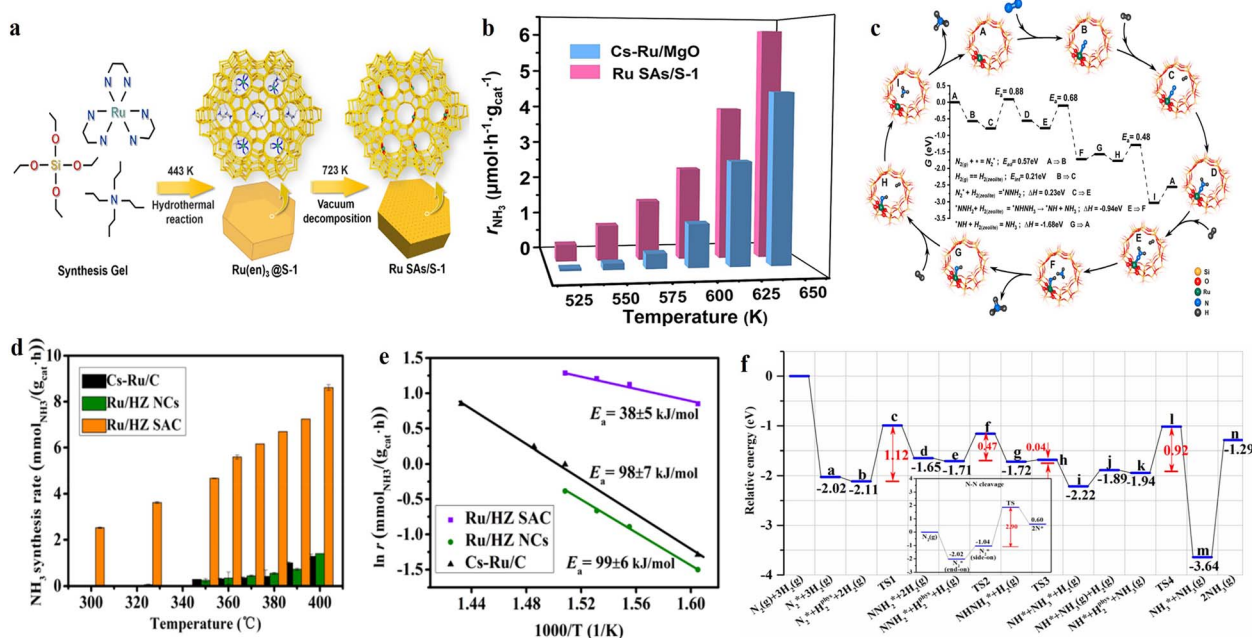


Fig. 2 (a) Synthesis procedure of Ru SAs/S-1. (b) Temperature dependence of  $\text{NH}_3$  synthesis rate over Ru SAs/S-1 and Cs–Ru/MgO varying from 523 to 648 K. (c) DFT calculation of  $\text{NH}_3$  synthesis reaction pathway over the Ru SAs/S-1 catalyst.<sup>63</sup> (d)  $\text{NH}_3$  synthesis rate and (e) Arrhenius plots of Ru/HZ SAC and Ru/HZ NCs catalysts as well as the Cs–Ru/C reference. (f) Potential energy diagrams for  $\text{NH}_3$  synthesis on Ru/HZ SAC via the formation of  $\text{NNH}_2^*$  as intermediates.<sup>65</sup>



value (0.36), which was different from the generally negative value for conventional Ru catalysts. DFT calculations indicated that  $N_2$  molecules can be linearly adsorbed in the exposed Ru single-atom active sites and reacted with  $H_2$  molecules physically adsorbed in the zeolite channels to form  $NH_3$  via a distal pathway of associative mechanism (Fig. 2c). Similarly, Li *et al.* employed HZSM-5 (HZ) zeolite with a rich microporous structure to serve as an anchoring site for stabilizing Ru single atoms (Ru/HZ SAC) by integrating a microwave single mode and ion exchange method.<sup>65</sup> Ru/HZ SAC with 0.2 wt% Ru exhibited excellent  $NH_3$  synthesis rate of  $4.67 \text{ mmol}_{NH_3} \text{ g}_{cat}^{-1} \text{ h}^{-1}$  at  $350^\circ\text{C}$  and 1 MPa, which was approximately 20-fold higher than that of Ru/HZ NCs (Fig. 2d). Moreover, the apparent activation energy for  $NH_3$  synthesis over Ru/HZ SAC ( $38 \text{ kJ mol}^{-1}$ ) (Fig. 2e) was significantly less than that of the conventional Ru-based catalysts ( $80\text{--}130 \text{ kJ mol}^{-1}$ ),<sup>66,67</sup> indicating the different reaction mechanism over the Ru/HZ SAC catalyst for  $NH_3$  synthesis. DFT calculations indicated that the direct dissociation of  $N_2$  into 2N on a single Ru site required a high energy barrier of 2.90 eV, while the hydrogenation via a distal pathway of associative mechanism to form  $^*NNH_2$  required only 1.12 eV (Fig. 2f), indicating that the dissociation adsorption pathway on Ru SACs was not favorable for  $NH_3$  synthesis.

## 2.2 Non-noble metal SACs

Compared with noble metal Ru-based catalysts, the development of non-noble metal single-atom catalysts are more attractive for industrial applications. Notably, carbon materials or N-doped carbon materials have been frequently reported as excellent supports for SACs due to their large specific surface area, tunable electronic structure, and electron transfer capability.<sup>68</sup> Wang *et al.* reported the N-doped carbon-supported Co SACs (Co-N-C) for  $NH_3$  synthesis under mild conditions.<sup>48</sup> At  $350^\circ\text{C}$  and 1 MPa, the  $NH_3$  synthesis rate of the Co-N-C catalyst was  $4.34 \text{ mmol}_{NH_3} \text{ g}_{cat}^{-1} \text{ h}^{-1}$ , which was 11- and 17-fold higher than that of Co/C and N-C, respectively (Fig. 3a). The outstanding performance of Co-N-C for  $NH_3$  synthesis was attributed to the synergistic effect of dynamic and steady-state dual-active sites. The stable  $Co_1-N_{3.5}$  active site formed by the coordination of Co with the pyrrolic N in the support facilitated the activation of  $N_2$  via the alternate pathway of associative mechanism, resulting in the stepwise hydrogenation to form  $^*HNNH$ ,  $^*NH-NH_3$ , and  $^*NH_2-NH_4$  species, followed by the cleavage of the N-N bond in  $^*NH_2-NH_4$  species to release  $NH_3$  (Fig. 3b). Moreover, the pyridine N species, which interacted less strongly with Co, can react with adsorbed  $H_2$  to form  $NH_3$  via a chemical looping pathway (Fig. 3c). To investigate the influence of different coordination environments

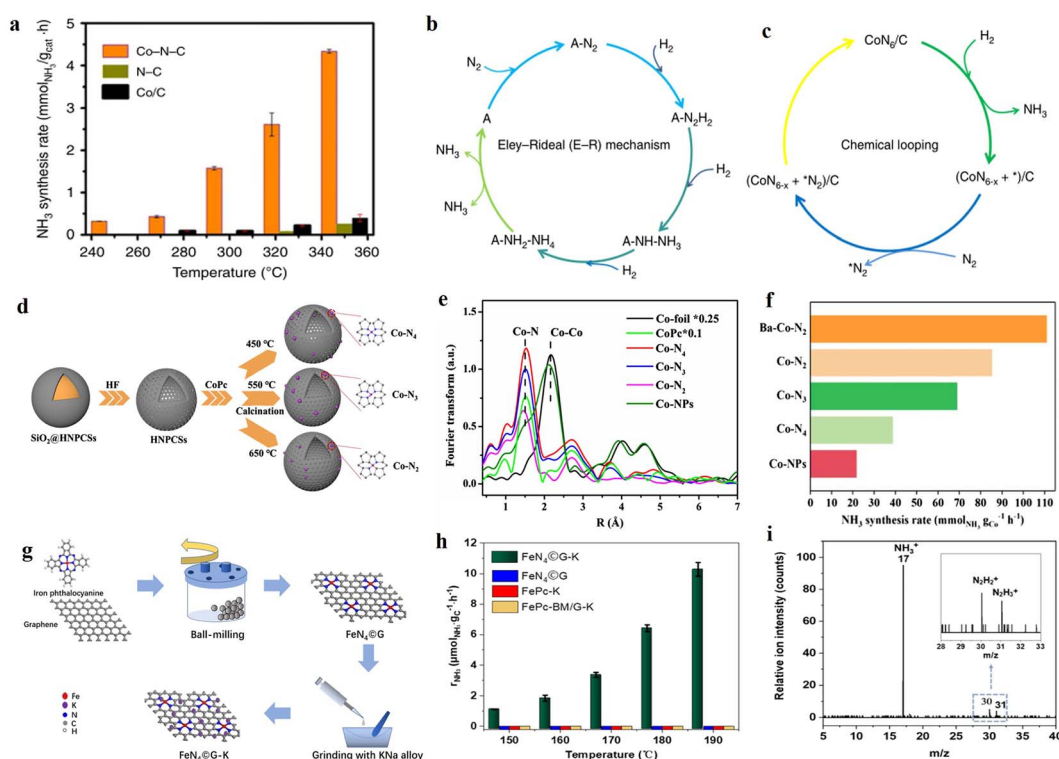


Fig. 3 (a)  $NH_3$  synthesis rate for Co-N-C, Co/C, and N-C under 1 MPa. (b)  $NH_3$  synthesis pathway on single Co sites in the form of steady-state  $Co_1-N_{3.5}$  (A represents the active sites); (c)  $NH_3$  production on dynamic cyclic sites via the chemical-looping pathway (x is in the range of  $0 < x \leq 1.5$  and  $V_N^*$  represents an anionic nitrogen vacancy).<sup>48</sup> (d) Schematic diagram of the preparation process of Co- $N_x$  with different CNs. (e) Co K-edge EXAFS spectra of Co- $N_x$  catalysts. (f)  $NH_3$  synthesis rate over the as-synthesized Co- $N_x$  catalysts at 1 MPa and  $300^\circ\text{C}$ . (g) Scheme for the preparation of the graphene lattice-confined Fe-single-site catalyst Fe $N_4$ @G-K. (h) Production rates of Fe $N_4$ @G-K, Fe $N_4$ @G, FePc-K, and FePc-BM/G-K as a function of reaction temperature at 0.1 MPa. (i) The effluents monitored by in  $NH_3$  synthesis over Fe $N_4$ @G-K at  $180^\circ\text{C}$ , 0.1 MPa, and WHSV of 30 L  $\text{g}_{cat}^{-1} \text{ h}^{-1}$ .

in SACs on  $\text{NH}_3$  synthesis performance, Zhou *et al.* prepared atomically dispersed Co-based catalysts with different Co–N coordination numbers by varying the pyrolysis temperatures.<sup>69</sup> With the increase in the pyrolysis temperature, the coordination number of Co–N decreased gradually. Co SACs with Co– $\text{N}_4$ , Co– $\text{N}_3$ , and Co– $\text{N}_2$  coordination structures were obtained at 450, 550 and 650 °C, respectively (Fig. 3d and e). Compared with Co– $\text{N}_4$  and Co– $\text{N}_3$  catalysts, the Co– $\text{N}_2$  catalyst with the lowest coordination number exhibited the best catalytic activity, with an  $\text{NH}_3$  synthesis rate of  $85.3 \text{ mmol}_{\text{NH}_3} \text{ g}_{\text{Co}}^{-1} \text{ h}^{-1}$  at 300 °C and 1 MPa (Fig. 3f). Various characterizations and DFT calculations elucidated that Co SAC with low coordination number could generate more unoccupied Co 3d charges and tetrahedral cobalt(II) sites, which can promote the electron transfer for  $\text{N}_2$  activation and the desorption N-containing intermediate species, respectively, thus resulting in a high  $\text{NH}_3$  synthesis rate. Similarly, Li *et al.* studied Co SACs with different Co–N coordination numbers and also showed that Co– $\text{N}_2$  catalysts with two coordination N atoms exhibited the best  $\text{NH}_3$  synthesis performance,<sup>70</sup> which was attributed to the fact that Co SACs with low Co–N coordination were conducive to  $\text{N}_2$  adsorption and activation.

In addition to Co-based single-atom catalysts, Fe- or Mo-based single-atom catalysts also exhibited excellent  $\text{NH}_3$  synthesis performance. Chen *et al.* successfully confined the  $\text{FeN}_4$  structure to the lattice of graphene by co-milling FePc and graphene at 450 rpm for 20 h (Fig. 3g).<sup>71</sup> The  $\text{FeN}_4\text{@G-K}$  catalyst with 24.5 wt% K showed an excellent catalytic activity under mild conditions, with  $\text{NH}_3$  synthesis rates of 1.1 and  $10.3 \text{ } \mu\text{mol}_{\text{NH}_3} \text{ g}_{\text{C}}^{-1} \text{ h}^{-1}$  at 150 °C and 190 °C, respectively (Fig. 3h). This study results revealed that the effective active site of the  $\text{FeN}_4\text{@G-K}$  catalyst for  $\text{N}_2$  activation was  $\text{FeN}_3$ , and  $\text{NH}_3$  was formed by gradual hydrogenation *via* an associative mechanism. Interestingly, the real-time detection of  $\text{N}_2\text{H}_2^+$  and  $\text{N}_2\text{H}_3^+$  intermediate species by time-of-flight mass spectrometer (TOF-MS) further experimentally verified the synthesis of  $\text{NH}_3$  by associative mechanism at the single atomic active site (Fig. 3i). Azofra *et al.* fabricated single Mo active sites confined in Si-based materials and applied it in the synthesis of  $\text{NH}_3$ .<sup>72</sup> At 400 °C and atmospheric pressure, the  $\text{NH}_3$  synthesis rate reached  $1.3 \text{ mmol g}_{\text{Mo}}^{-1} \text{ h}^{-1}$ . Theoretical calculations indicated that  $\text{N}_2$  spontaneously adsorbed and was activated on the  $[(\equiv\text{Si-O})\text{MoH}_3]$  site *via* an associative mechanism, where the rate-determining step is the further hydrogenation of the adsorbed  $^*\text{NHNH}_2$  to form  $\text{NH}_3$ .

In summary, SACs possess a unique geometric and electronic structure as well as complete metal dispersion compared with nanoparticle catalysts. The single-atom sites over SACs cannot realize the direct dissociation of  $\text{N}_2$  while enabling  $\text{N}_2$  activation *via* an associative route for  $\text{NH}_3$  synthesis. The distinct reaction mechanism on SACs in comparison with nanoparticle catalysts is conducive to realizing higher  $\text{NH}_3$  synthesis rate at mild conditions. Nevertheless, the disadvantages of SACs for  $\text{NH}_3$  synthesis are also obvious. On the one hand, due to the high surface free energy, the single atoms are easy to migrate and agglomerate. Moreover, the metal loading of SACs is generally low, which limits the catalytic activity of  $\text{NH}_3$  synthesis. On the other hand, it is difficult for a single-atom active site to activate both  $\text{N}_2$  and  $\text{H}_2$  molecules at the

same time, which may result in hydrogen poisoning phenomena, such as the observation of negative  $\text{H}_2$  reaction order in  $\text{Ru}_1/\text{CeO}_2$ .<sup>73</sup> Therefore, developing high-loading SACs or combining single atoms with other active centers are effective strategies to further improve the  $\text{NH}_3$  synthesis performance.

### 3. SCCs for $\text{NH}_3$ synthesis

Unlike SACs where single atoms are highly dispersed on the support in isolation, a number of atoms assembled in the form of individual clusters can form single-cluster catalysts, which results in unique geometric and electronic structure. The cluster catalysts can not only provide multiple metal atoms as catalytic sites but also possess high metal dispersion. The single-cluster catalyst can be simply classified as noble metal SCCs and non-noble metal SCCs.

#### 3.1 Noble metal SCCs

It is well known that  $\text{NH}_3$  synthesis is a size-sensitive reaction, where the size of Ru has a significant impact on the activity of  $\text{NH}_3$  synthesis. According to DFT calculation based on the model of Wulff construction, when the particle size was between 1.8 and 2.5 nm, the number of Ru  $\text{B}_5$  sites was enriched, which was conducive to the adsorption and dissociation of  $\text{N}_2$ .<sup>33</sup> Jacobsen *et al.* also indicated that the optimal Ru particle size was approximately 2 nm, which can maximize the proportion of  $\text{B}_5$  sites to improve  $\text{NH}_3$  synthesis performance. When the size of Ru particle was less than 2 nm, the proportion of corner sites increased along with the decreased in the number of  $\text{B}_5$  sites. Therefore, previous research predicted that the small Ru clusters in the absence of  $\text{B}_5$  sites were supposed to be inactive in  $\text{NH}_3$  synthesis.<sup>74</sup>

Nevertheless, recent studies have shown that the activity of  $\text{NH}_3$  synthesis increases with the decrease in Ru particle size. For instance, Zhou *et al.* synthesized a series of  $\text{Ru}/\text{BaCeO}_3$  catalysts with various Ru particle sizes (1.1–3.0 nm) using size-controlled Ru colloids as precursors.<sup>75</sup> The experimental results showed that the  $\text{NH}_3$  synthesis rate significantly increased as the Ru particle size decreased from 3.0 nm to 1.1 nm. At 400 °C and 1 MPa, the  $\text{TOF}_{\text{Ru total}}$  of  $\text{Ru1.1}/\text{BaCeO}_3$  can reach up to  $0.124 \text{ s}^{-1}$ , which was about 6-fold higher than that of  $\text{Ru3.0}/\text{BaCeO}_3$  (Fig. 4a). It was revealed that the small Ru clusters were conducive to the formation of  $\text{Ce}^{3+}$  and  $\text{O}_v$  species in  $\text{BaCeO}_3$ , which promoted the electron transfer from Ru metal to  $\text{N}_2$ , thereby accelerating the dissociation of  $\text{N}_2$ . In addition, the small Ru clusters enhanced hydrogen spillover from Ru to  $\text{BaCeO}_3$  support to alleviate hydrogen poisoning, resulting in efficient  $\text{NH}_3$  synthesis. Similarly, Peng *et al.* used N-doped carbon as a carrier and prepared a series of Ru catalysts with sizes ranging from 1.4 to 5.0 nm using colloidal Ru deposition method.<sup>19</sup> The study found that the TOF of 5 nm Ru NPs was  $2.53 \times 10^{-2} \text{ s}^{-1}$ . When the particle size decreased from 5.0 nm to 1.4 nm, the TOF increased to  $5.23 \times 10^{-2} \text{ s}^{-1}$ , mainly due to the increase in the corner sites of the catalyst (Fig. 4b), which was beneficial for reducing the work function and promoting  $\text{N}_2$  activation. These results unravel the size-dependent effect of





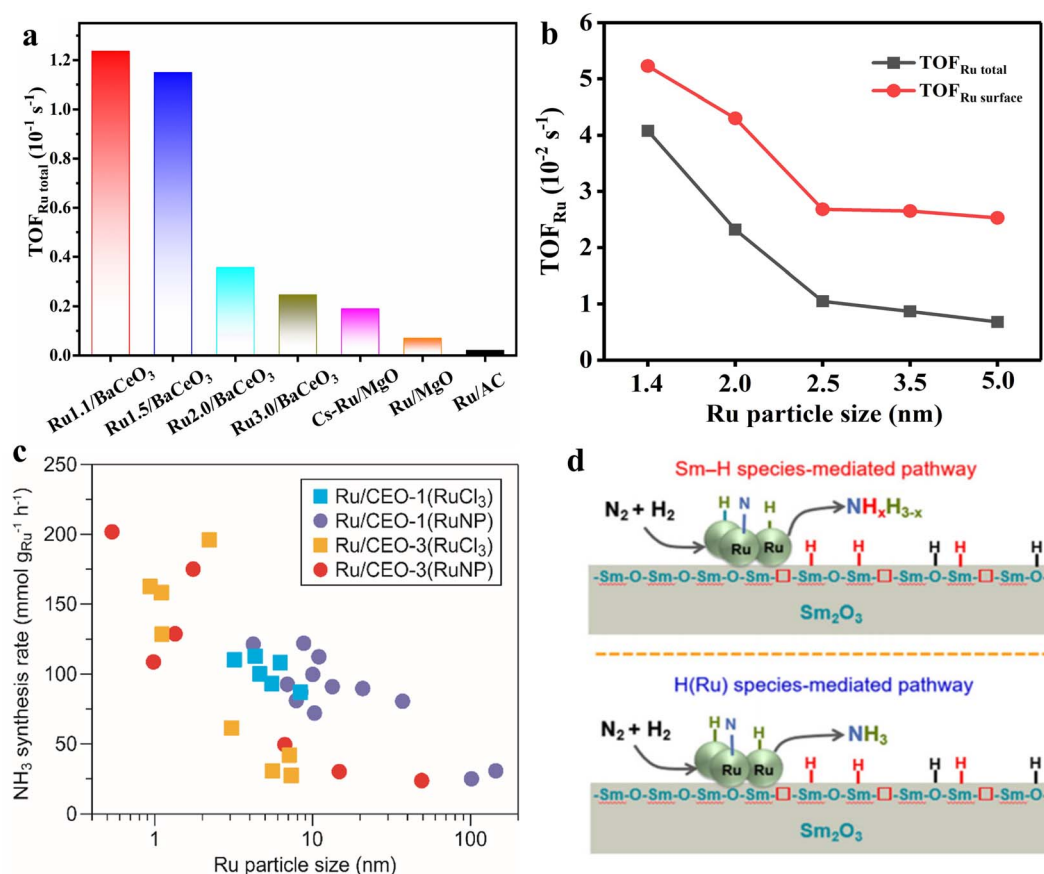


Fig. 4 (a) TOF<sub>Ru total</sub> of the Ru<sub>x</sub>BeCeO<sub>3</sub> catalysts at 400 °C and 1 MPa.<sup>75</sup> (b) TOF<sub>Ru</sub> of Ru NCs at 400 °C and 1 MPa.<sup>19</sup> (c) NH<sub>3</sub> synthesis rate of Ru/CEO-1 and Ru/CEO-3 catalysts at 400 °C and 0.1 MPa as a function of the mean Ru particle size.<sup>80</sup> (d) Schematic illustration of chemisorbed H(Ru) species-mediated and Sm-H species-mediated reaction pathways on the Ru/Sm<sub>2</sub>O<sub>3</sub> catalyst. Color code for different kinds of H species: H(Ru), Sm-H and O-H species are shown in blue, red and black, respectively.<sup>81,82</sup>

Ru-based catalysts and highlight the superior activity of Ru cluster catalysts in NH<sub>3</sub> synthesis.

In recent years, an increasing number of Ru cluster catalysts have been reported to exhibit high NH<sub>3</sub> synthesis performance. Li *et al.* found that the activity of Ru/MgO-MIL with small Ru clusters (1.0 nm) in NH<sub>3</sub> synthesis was approximately 19 times that of traditional 2–4 nm Ru/MgO catalyst and 7.7 times that of Ru@MIL-101.<sup>76</sup> The superior mass activity was largely due to the efficient utilization of Ru atomic clusters. Meanwhile, the authors believed that the theoretical model of Ru particles was based on the Wulff construction, while under realistic conditions, small clusters might deviate from the ideal thermodynamic model and generate B<sub>5</sub> sites on the surface.<sup>77,78</sup> Feng *et al.* synthesized CeO<sub>2</sub> nanorods-supported subnano Ru clusters for NH<sub>3</sub> synthesis at mild conditions.<sup>79</sup> The Ru clusters/CeO<sub>2</sub> exhibited a much higher activity in NH<sub>3</sub> synthesis than the Ru nanoparticle counterpart. It was revealed that the subnanometer Ru clusters species facilitated the activation and dissociation of H<sub>2</sub> and N<sub>2</sub> molecules, mainly responsible for its intrinsic activity in NH<sub>3</sub> synthesis. Similarly, Hirabayashi *et al.* also found that the Ru small clusters over Ru/CeO<sub>2</sub> exhibited a superior NH<sub>3</sub> synthesis performance (Fig. 4c).<sup>80</sup> Furthermore, the Sm<sub>2</sub>O<sub>3</sub>-supported sub-nanometer Ru cluster catalyst was

developed and exhibited superior NH<sub>3</sub> synthesis performance. Mechanistic studies and theoretical calculations showed that for the activated Ru/Sm<sub>2</sub>O<sub>3</sub>, a large amount of surface Sm-H species could be generated on Sm<sub>2</sub>O<sub>3</sub> (Fig. 4d). The Sm-H species not only can cooperate with Ru clusters to reduce the energy barrier of nitrogen dissociation but also can directly participate in the formation of NH<sub>3</sub> on Ru clusters.<sup>81,82</sup>

Theoretical calculations in recent years also support the idea that cluster catalysts promote NH<sub>3</sub> synthesis more effectively. Taking the Ru<sub>3</sub> clusters as an example, Wang *et al.* investigated the Ru<sub>3</sub> single clusters anchored on the defective g-C<sub>3</sub>N<sub>4</sub> nanosheet (Ru<sub>3</sub>/Nv-g-C<sub>3</sub>N<sub>4</sub>) for NH<sub>3</sub> synthesis based on DFT calculations and microscopic kinetic simulations.<sup>83</sup> Under the industrial reaction conditions of NH<sub>3</sub> synthesis at 673 K and 100 bar, the TOF of Ru<sub>3</sub>/Nv-g-C<sub>3</sub>N<sub>4</sub> is 5.8 times that of the Ru (0001) step surface. DFT calculations revealed that the reaction proceeded parallelly on Ru<sub>3</sub>/Nv-g-C<sub>3</sub>N<sub>4</sub> through both dissociative and alternative associative mechanisms. With increasing temperatures or decreasing pressures, the dissociative mechanism gradually prevailed and the associative mechanism receded (Fig. 5a and b). Furthermore, Cheng used Ru<sub>19</sub> clusters as an example to calculate the free energy distribution of a typical catalytic reaction<sup>84</sup> based on *ab initio* molecular



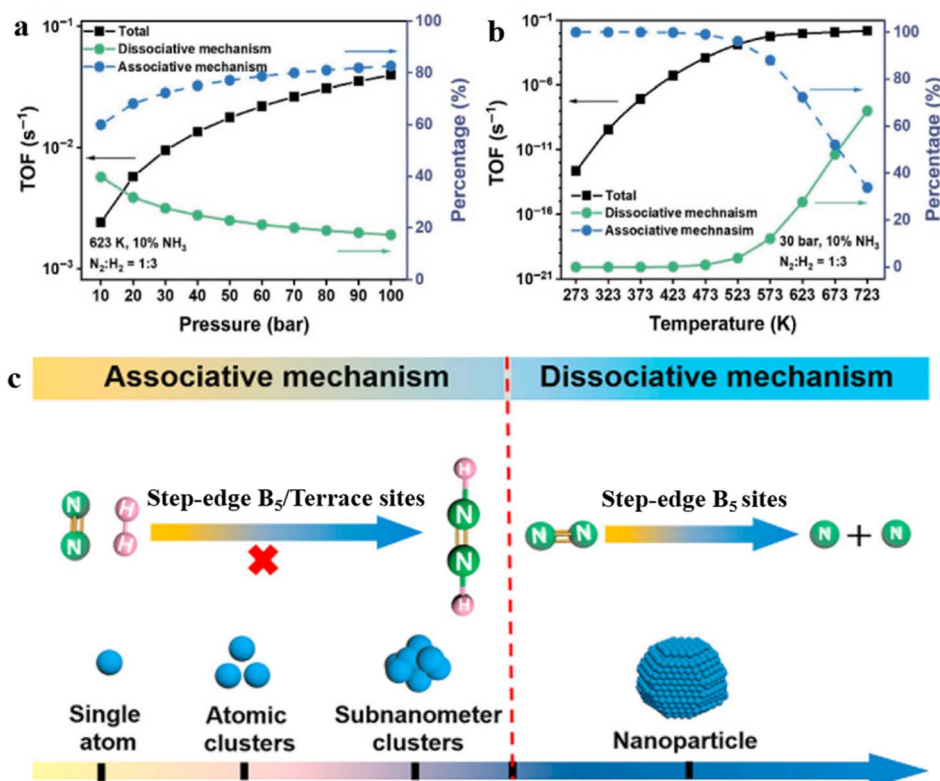


Fig. 5 TOFs and contributions from dissociative and associative mechanisms as functions of (a) pressure under constant temperature of 623 K, (b) temperature under constant pressure of 30 bar.<sup>83</sup> (c) NH<sub>3</sub> synthesis pathway over Ru catalysts with different sizes.<sup>49</sup>

dynamics (AIMD) and free energy methods. It was found that the reaction free energies (DrG) and barrier (DGa) of the Ru<sub>19</sub> clusters were quite different from those obtained from static geometric optimization methods, indicating that the dynamic fluctuations of clusters configurations significantly affected the reaction free energy and potential barrier. Notably, the phase transition of sub-nanometer clusters can accelerate the N<sub>2</sub> activation due to the reduction of reaction free energy and enabling NH<sub>3</sub> synthesis at low temperatures.

Due to the absence of Ru B<sub>5</sub> sites over Ru clusters, the reaction mechanism over Ru clusters may be different from Ru nanoparticle catalysts. Zhou *et al.* reported the design of sub-nanocluster Ru clusters (0.8 nm) anchored on hollow N-doped carbon spheres (Ru-SNCs) catalysts.<sup>85</sup> Under 400 °C and 3 MPa conditions, the TOF<sub>Ru</sub> of 0.5Ru-SNC (0.067 s<sup>-1</sup>) was 3.5 times higher than that of the 1.2Ru-NPs catalyst (0.019 s<sup>-1</sup>). The UV-vis and *in situ* infrared experiments showed that the N<sub>2</sub>H<sub>4</sub> species was the main intermediate for NH<sub>3</sub> synthesis on the Ru-SNCs catalyst. It demonstrated that the Ru-SNCs catalyst can follow an associative route for N<sub>2</sub> activation, which circumvented the direct dissociation of N<sub>2</sub> and resulted in highly efficient NH<sub>3</sub> synthesis at mild conditions. Furthermore, Li *et al.* synthesized a series of Ru catalysts with Ru sizes ranging from single atoms, atomic clusters, sub-nanometric clusters, to nanoparticles.<sup>49</sup> Researches showed that with the size decrease of Ru nanoparticle to sub-nanometric and atomic level, the activation pathway of N<sub>2</sub> changed from dissociative mechanism

to associative mechanism (Fig. 5c). At the sub-nanometric level, the enhanced intra-cluster interaction of atomic clusters upshifted the Ru d-band center toward the Fermi level, thus significantly promoting N<sub>2</sub> activation *via* the associative mechanism with extremely small reaction energy barriers. In addition, the synergistic effect of single atom and cluster for NH<sub>3</sub> synthesis was investigated. Sivan *et al.* synthesized a series of Ru single atoms, clusters, and nanoparticles using a one-pot method to study the effect of Ru size on NH<sub>3</sub> synthesis.<sup>86</sup> The order of TOF was as follows: 2.8Ru-CeO<sub>2</sub> (Ru single atom and cluster) > 1.4Ru-CeO<sub>2</sub> (Ru single atom) > 4.0Ru-CeO<sub>2</sub> (Ru nanoparticle) > 5.3Ru-CeO<sub>2</sub> (Ru nanoparticle). It was suggested that the 2.8Ru-CeO<sub>2</sub> catalyst, which contained both Ru single atoms and clusters, can trigger NH<sub>3</sub> synthesis through the integration of dissociative and associative routes, resulting in excellent catalytic activity and stability. This work indicates that the combination of Ru single atom and cluster is a promising strategy to improve NH<sub>3</sub> synthesis performance.

In summary, recent researches have shown that the Ru cluster catalysts usually exhibit higher NH<sub>3</sub> synthesis rates than Ru nanoparticle catalysts. The potential reasons are summarized as follow: (1) the Ru cluster catalysts possess a higher metal dispersion and utilization than Ru nanoparticle catalysts; (2) the strong intra-cluster interaction of the Ru cluster can enhance the adsorption and activation of N<sub>2</sub> molecules; (3) the distinct reaction mechanism over Ru cluster catalysts compared with Ru nanoparticle catalysts enables facile NH<sub>3</sub> synthesis





under mild conditions. Nevertheless, the associative mechanism over Ru cluster catalysts is still controversial, which still require solid evidence to support this opinion. Therefore, there is an urgent need to develop more advanced characterization techniques such as time-of-flight secondary ion mass spectrometry (TOF-SIMS) and neutron technology to detect intermediate species and elucidate the reaction mechanism.

### 3.2 Non-noble metal SCCs

Theoretical calculations indicate that an ideal metal catalyst for  $\text{NH}_3$  synthesis should have moderate adsorption energy of N atoms and  $\text{NH}_x$  desorption energy, namely, near the top position of the volcano diagram, such as the Ru metal.<sup>87,88</sup> In consideration of the scarcity and high price of Ru metal, there is an urgent need to develop catalysts with excellent catalytic performance, cost-effective or rich in Earth for  $\text{NH}_3$  synthesis at mild conditions.<sup>89</sup> Liu *et al.* proposed an active center of  $\text{Fe}_3$  clusters anchored on the  $\text{Al}_2\text{O}_3$  (010) surface through first-principles calculations and microkinetic analysis (Fig. 6a).<sup>47</sup> The study found that the first hydrogenation of  $\text{N}_2$  to generate  $\text{NNH}$  on the  $\text{Fe}_3/\theta\text{-Al}_2\text{O}_3$  (010) surface was much faster than the dissociative mechanism. The subsequent  $\text{NNH}$  dissociation also had a low energy barrier of 0.45 eV, thus bypassing the BEP relationship and the limitation on one the side of the volcano curve (Fig. 6b). Correspondingly, the calculated TOF of  $\text{NH}_3$  synthesis on  $\text{Fe}_3/\theta\text{-Al}_2\text{O}_3$  (010) was comparable to that of Ru  $\text{B}_5$  sites and was two orders of magnitude faster than the  $\text{C}_7$  sites of Fe. These results indicated that surface-anchored metal trimers and/or multinuclear clusters might serve as efficient catalysts for  $\text{NH}_3$  synthesis at mild conditions. Meanwhile, Luo *et al.* conducted a systematic study of  $\text{NH}_3$  synthesis on triatomic metal clusters ( $\text{M}_3$ ) of 20 transition metals.<sup>90</sup> The three key processes including  $\text{N}_2$  dissociation, hydrogenation, and  $\text{NH}_3$  desorption were calculated to evaluate the catalytic roles of

these  $\text{M}_3$  clusters. The results showed that the transition metals can be divided into three categories (Fig. 6c): (1)  $\text{N}_2$  can spontaneously dissociate on TMI- $\text{M}_3$  metals (*i.e.*,  $\text{Sc}_3$ ,  $\text{Ti}_3$ ,  $\text{V}_3$ ,  $\text{Y}_3$ ,  $\text{Zr}_3$ , and  $\text{Nb}_3$ ); (2) obvious activation barriers needed to be overcome on TMII- $\text{M}_3$  metal clusters (*i.e.*,  $\text{Cr}_3$ ,  $\text{Mn}_3$ ,  $\text{Fe}_3$ ,  $\text{Co}_3$ ,  $\text{Mo}_3$ ,  $\text{Tc}_3$ ,  $\text{Ru}_3$ , and  $\text{Rh}_3$ ); (3) and the activation process on TMIII- $\text{M}_3$  clusters (*i.e.*,  $\text{Ni}_3$ ,  $\text{Cu}_3$ ,  $\text{Zn}_3$ ,  $\text{Pd}_3$ ,  $\text{Ag}_3$ , and  $\text{Cd}_3$ ) was not feasible. Considering the three key processes for  $\text{N}_2$  reduction to  $\text{NH}_3$ , four  $\text{M}_3$  clusters in the TMI group ( $\text{Y}_3$ ,  $\text{Sc}_3$ ,  $\text{Zr}_3$ , and  $\text{Nb}_3$ ) were proposed as ideal candidate clusters catalyst for  $\text{NH}_3$  synthesis.

Beyond theoretical calculations, Peng *et al.* conducted research on the synthesis of  $\text{NH}_3$  using non-precious metal cluster catalysts.<sup>20</sup> The cobalt atomic dimers on a nitrogen-carbon support ( $\text{Co}_2$  ACCs) were synthesized for  $\text{NH}_3$  synthesis and using the Co SAC and Ru NPS as references. Under 400 °C and 1 MPa,  $\text{Co}_2$  ACCs exhibited a very high  $\text{NH}_3$  synthesis rate of  $8.54 \text{ mmol}_{\text{NH}_3} \text{ g}_{\text{cat}}^{-1} \text{ h}^{-1}$ , which is  $\sim 1.8$ - and  $3.3$ -fold that of the Co SAC ( $4.60 \text{ mmol}_{\text{NH}_3} \text{ g}_{\text{cat}}^{-1} \text{ h}^{-1}$ ) and Co NPs ( $2.55 \text{ mmol}_{\text{NH}_3} \text{ g}_{\text{cat}}^{-1} \text{ h}^{-1}$ ), respectively. The low  $\text{N}_2$  reaction order and the bands associated with  $\text{N}_2\text{H}_x$  intermediates in the *in situ* diffuse reflectance infrared Fourier-transform spectroscopy (DRIFTS) suggested that  $\text{N}_2$  was not directly dissociated while it underwent the associative route for  $\text{NH}_3$  synthesis (Fig. 6d and e).

Although there is currently limited research on non-precious metal cluster catalysts in  $\text{NH}_3$  synthesis, theoretical studies indicate that non-precious metal cluster catalysts exhibit significant potential in this regard. The key challenge is to prepare uniform non-precious metal cluster catalysts with a specific number of atoms. Current methods for preparing atomic clusters include (1) using precursors containing specific atomic clusters; (2) anchoring atomic clusters on carrier materials with defect sites, such as  $\text{C}_3\text{N}_4$  carriers; and (3) the application of atomic layer deposition (ALD). Besides, developing more efficient methods for preparing atomic cluster catalysts is of great significance.

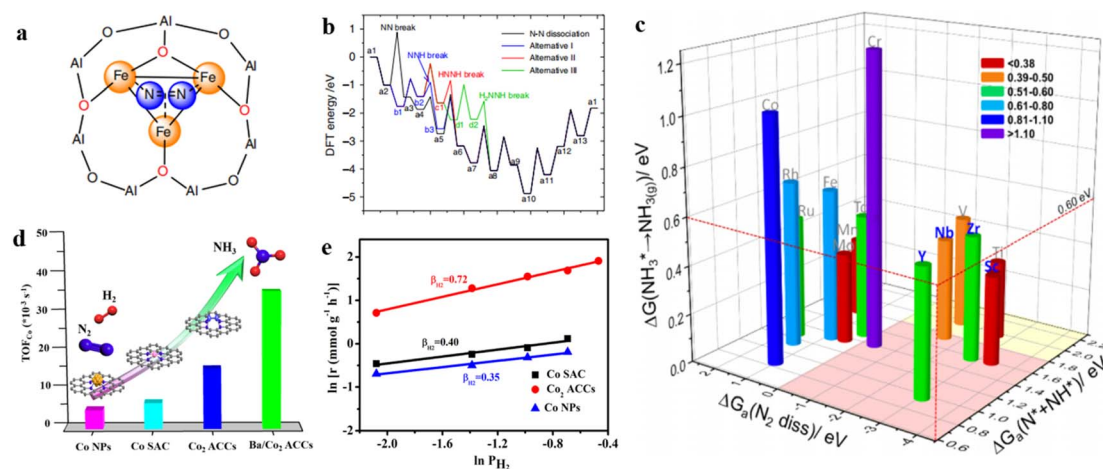


Fig. 6 (a) Schematic representation of  $\text{N}_2$  coordinated with heterogeneous  $\text{Fe}_3/\theta\text{-Al}_2\text{O}_3(010)$  in the same configuration; (b) the dissociative mechanism, and three pathways of associative mechanism with N-N bond dissociation at  $\text{*NNH}$ ,  $\text{*HNNH}$ , and  $\text{*HNNH}_2$  intermediates by the alternating hydrogenation route.<sup>47</sup> (c) Summary of the free energy of transition state for  $\text{N}_2$  dissociation, hydrogenation barrier of  $\text{*N} + \text{*NH}$  formation, and desorption energy of  $\text{NH}_3$  on 14 three-atom metal clusters.<sup>90</sup> (d) Turnover frequencies ( $\text{TOF}_{\text{Co total}}$ ) at 400 °C and 1 MPa. (e) Reaction orders of  $\text{H}_2$  over different catalysts at 400 °C and 1 MPa.<sup>20</sup>



## 4. BCCs for $\text{NH}_3$ synthesis

Apart from single-atom and single-cluster catalysts, bimetallic clusters have emerged as one of the important categories of heterogeneous catalyst. In many cases, bimetallic catalysts exhibit higher catalytic activity or selectivity than their monometallic counterpart due to the strong synergistic effect between different sites.<sup>91,92</sup> In  $\text{NH}_3$  synthesis, it was reported that the dual-site strategy can effectively improve  $\text{NH}_3$  synthesis performance owing to the separated sites for  $\text{N}_2$  and  $\text{H}_2$  activation, which can not only avoid the hydrogen poisonous over active sites caused by competition adsorption of  $\text{N}_2$  and  $\text{H}_2$ , but also provide the possibility to circumvent the scale relations in  $\text{NH}_3$  synthesis.<sup>93,94</sup> In addition, the bimetallic-cluster catalysts exhibit quite distinct properties in electronic and geometric structure compared with monometallic catalysts, which has a great impact on the reaction mechanism in  $\text{NH}_3$  synthesis.<sup>95</sup> In general, according to the composition and structure of bimetallic catalysts, it can be classified into bimetallic-alloy catalysts, bimetallic single-cluster catalysts, and single-atom/dimer alloy catalysts.

### 4.1 Bimetallic-alloy catalysts

Because of high surface free energy, the Ru clusters are thermodynamically unstable and tend to sinter at high temperatures during  $\text{NH}_3$  synthesis. In order to increase the stability of Ru clusters, Ni *et al.* reported a method to confine  $\text{Co}_x\text{Ru}_y$

nanoparticles in the pores of N-doped carbon through the guiding of benzoic acid to restrict the deposition location of Ru and Co species.<sup>96</sup> The results of high-angle annular dark field scanning transmission electron microscopy (HAADF-STEM) showed that the  $\text{Co}_x\text{Ru}_y$  alloy with an average size of 2.2–2.6 nm was confined inside the pores of N-doped carbon spheres. The catalytic activity test displayed that  $\text{Co}_1\text{Ru}_2/\text{NC}$  had a high  $\text{NH}_3$  synthesis rate of  $18.9 \text{ mmol}_{\text{NH}_3} \text{ g}_{\text{cat}}^{-1} \text{ h}^{-1}$  at 400 °C and 3 MPa, which is 3.2-fold that of the Ru/NC catalyst (Fig. 7a). In addition,  $\text{Co}_1\text{Ru}_2/\text{NC}$  presented a relatively higher stability in  $\text{NH}_3$  synthesis than  $\text{Co}_1\text{Ru}_2/\text{NC-IWI}$  prepared by traditional incipient wetness impregnation method (Fig. 7b), demonstrating that the confinement of Ru and Co NPs inside the hollow pores of N-doped carbon spheres can enhance the stability of RuCo alloy. In comparison with Ru-Co nanoparticles, Yang *et al.* developed a bimetallic Ru-Co clusters/N-C catalyst derived from a confined alloying process within zeolite-imidazolate frameworks (ZIF).<sup>97</sup> As shown in Fig. 7c,  $\text{Ru}_3(\text{CO})_{12}$  was introduced into the cavity of ZIFs that use the Co-bearing metal-organic frameworks as the host. After decomposition at 900 °C, the bimetallic Ru-Co clusters can be *in situ* formed. Fig. 7d showed that Ru-Co clusters@N-C possessed the highest  $\text{NH}_3$  synthesis rate among Ru-Co NPs@N-C, Ru clusters@N-C, and Ru NPs@N-C catalysts. Compared with the Ru-Co NPs catalyst, the bimetallic Ru-Co clusters exhibited a higher density of low-coordination and unsaturated active sites, which may favor the adsorption and activation of  $\text{N}_2$  molecules.

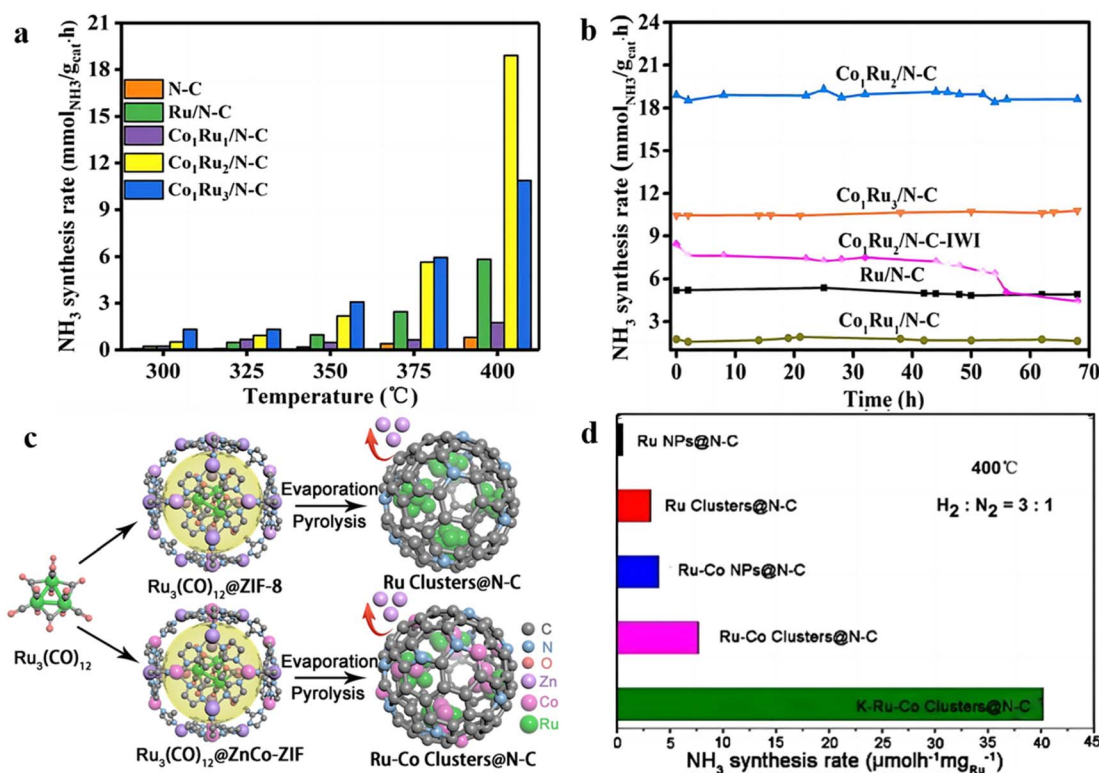


Fig. 7 (a)  $\text{NH}_3$  synthesis rate over catalysts at 300–400 °C and 3 MPa. (b) Time dependence of  $\text{NH}_3$  synthesis rate at 400 °C and 3 MPa.<sup>96</sup> (c) Schematic diagram of the preparation of Ru-Co clusters@N-C catalyst. (d)  $\text{NH}_3$  synthesis rate over the as-prepared catalysts at 400 °C and 0.1 MPa.<sup>97</sup>



Besides, alloying with Co atoms would tailor the local structure of Ru clusters owing to the synergistic effect. As a result, the  $\text{NH}_3$  synthesis rate over Ru–Co clusters@N–C is 2.4 times higher than that of Ru clusters@N–C. These results elucidate that bimetallic Ru–Co alloy can not only improve  $\text{NH}_3$  synthesis rate but also increase the thermal stability compared with Ru nanoparticle catalysts.

## 4.2 Bimetallic single-cluster catalysts

Bimetallic single-cluster catalysts mean that one of the elements in bimetallic clusters is atomically dispersed.<sup>98,99</sup> The bimetallic single-cluster sites ( $\text{M}_1\text{A}_n$ ) not merely possess the advantage of SACs with complete metal dispersion but also provide the possibility to overcome scaling relation through the cooperative effects of bimetallic sites that are responsible for different elementary steps. In  $\text{NH}_3$  synthesis, Ma *et al.* explored the reaction mechanism of  $\text{N}_2$ -to- $\text{NH}_3$  thermal conversion on the bimetallic  $\text{Rh}_1\text{Co}_3$  site using DFT calculation.<sup>100</sup> They found that the preferred reaction pathway over the  $\text{Rh}_1\text{Co}_3$  site was the associative mechanism analogous to the biological process, which was driven by both the charge buffering ability of doped metal Rh in  $\text{Rh}_1\text{Co}_3$  and the complementary role of Co in catalysis (Fig. 8a). Apart from the bimetallic single-cluster anchored on a metal oxide, the supported bimetallic single-cluster catalysts are also promising for  $\text{NH}_3$  synthesis. Ru-loaded hydrides were reported to work as efficient catalysts

for  $\text{NH}_3$  synthesis at low temperatures, where the formation of hydrogen vacancies ( $\text{V}_\text{H}$ ) at the Ru/hydrides is a key factor for  $\text{NH}_3$  synthesis. Nakao *et al.* investigated the  $\text{V}_\text{H}$  formation and H-migration behavior at the Ru-TM/ $\text{Ca}_2\text{NH}$  interface using the  $\text{Ru}_5\text{TM}/\text{Ca}_2\text{NH}$  model by DFT calculations (Fig. 8b).<sup>101</sup> It was revealed that the five late TMs (Fe, Co, Rh, Os, and Ir) and eight early TMs (Sc, Ti, Y, Zr, Nb, La, Hf, and Ta) were determined to promote  $\text{V}_\text{H}$  formation. In addition, Nb, Hf, Ta, Os, and Ir can also decrease the H-migration energy at the  $\text{Ru}_5\text{TM}/\text{Ca}_2\text{NH}$  interface when compared with that at the  $\text{Ru}_6/\text{Ca}_2\text{NH}$  interface. Therefore, the formation of bimetallic  $\text{Ru}_5\text{TM}$  clusters over hydrides *via* the addition of a proper TM atom can improve the  $\text{NH}_3$  synthesis performance in terms of the  $\text{V}_\text{H}$  formation and H-migration energy. To unveil the synergy of bimetallic sites, Cheng *et al.* studied the  $\text{Fe}_{13}$  cluster and bimetallic  $\text{Fe}_{12}\text{X}$  ( $\text{X} = \text{V}, \text{Cr}, \text{Mn}, \text{Co}, \text{Ni}, \text{Cu}, \text{Zn}, \text{Nb}, \text{Mo}, \text{Ru}, \text{and Rh}$ ) clusters for  $\text{NH}_3$  synthesis (Fig. 8c).<sup>102</sup> The energies analysis showed that center substitution ( $\text{X}@\text{Fe}_{12}$ ) was favored while doping single V, Cr, Co, and Mo atoms, whereas Mn, Ni, Cu, Zn, Nb, Ru, and Rh tended to form shell-doped structures ( $\text{Fe}_{12}\text{X}$ ). Among these bimetallic single clusters,  $\text{Fe}_{12}\text{Nb}$  exhibited the lowest activation energy for  $\text{N}_2$  dissociation and the dissociated  $^*\text{N}$  species was converted into  $\text{NH}_3$  efficiently *via* a hydrogenation process (Fig. 8d).

To be noted, although bimetallic single-cluster catalysts show great advantages for  $\text{NH}_3$  synthesis on the basis of DFT calculations, the synthesis and application of bimetallic single-cluster catalysts in  $\text{NH}_3$  synthesis have not been reported yet.

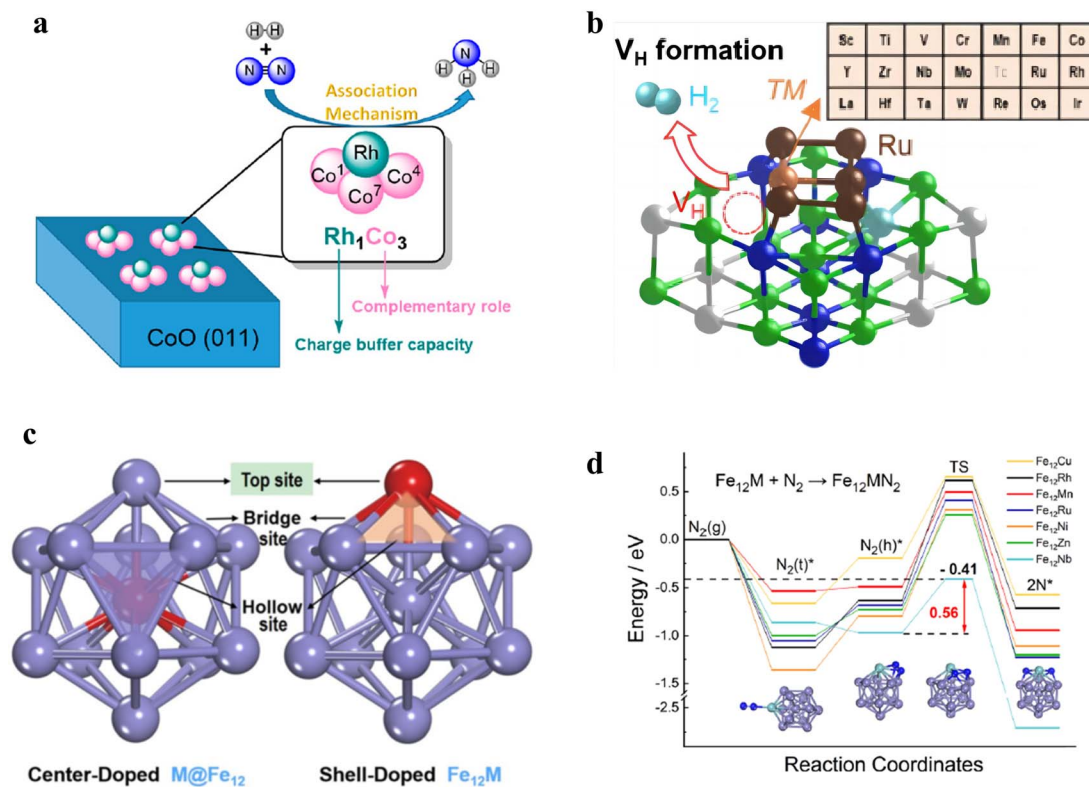


Fig. 8 (a) Schematic diagram of  $\text{Rh}_1\text{Co}_3$  bimetallic sites for  $\text{NH}_3$  synthesis.<sup>100</sup> (b) Schematic diagram of the  $\text{Ru}_5\text{TM}/\text{Ca}_2\text{NH}$  model.<sup>101</sup> (c) The chemical structure of heteroatom-doped  $\text{Fe}_{13}$  clusters. The red atoms represent the different doping positions.<sup>102</sup> (d) Pathways of  $\text{N}_2$  adsorption and dissociation on the shell-doped  $\text{Fe}_{12}\text{TM}$  clusters.



The main challenge lies in the preparation of uniform bimetallic clusters with specific structure, which requires the development of special preparation method and the application of advanced equipment. Besides, DFT calculations demonstrated that the reaction mechanism of  $\text{NH}_3$  synthesis over bimetallic single-cluster catalysts is closely related to their composition and property. For instance, the preferred reaction pathway over the  $\text{Rh}_1\text{Co}_3$  site is an associative mechanism, while that over the  $\text{Fe}_{12}\text{X}$  ( $\text{X} = \text{Mn}, \text{Ni}, \text{Cu}, \text{Zn}, \text{Nb}, \text{Ru}, \text{and Rh}$ ) site is dissociative mechanism. The real reaction mechanisms over different bimetallic single-cluster catalysts still need to be further confirmed by experimental research.

### 4.3 Single-atom/dimer alloy catalysts

Single-atom alloys (SAAs) are a class of bimetallic single-site heterogeneous catalyst in which small amounts of one metal are atomically dispersed in the surface of a different metal.<sup>103,104</sup> Distinguished from traditional metal alloy, the amount of guest metal atom in SAAs is small and the sites are isolated. Due to the unique geometry of SAAs, the location of the transition state and the binding site of reaction intermediates are often decoupled, which make it possible to enable both the facile dissociation of reactants and weak binding of the intermediates. For example, Zhang *et al.* reported a  $\text{Co}_1\text{Ru}$  SAA catalyst *via* the deposition of atomically dispersed Co onto the surface of Ru tiny subnanoclusters (TCs).<sup>105</sup> It was revealed that the special structure can generate a spatial effect and induce strong inter-electronic interactions between Ru and Co, which can lead to

the simultaneous generation of the high-surface-unoccupied Co 3d charge and obvious upshifting of the Ru d-band center. Based on the special electronic and geometric structure,  $\text{Co}_1\text{Ru}$  TCs can promote  $\text{N}_2$  activation with a low barrier energy and enable the repulsion to the adsorption of the N-containing intermediates on the catalyst surface, resulting in the weakening of the binding of  $^*\text{NH}_3$  and  $^*\text{N}_2\text{H}_4$  intermediates on the  $\text{Co}_1\text{Ru}$  TCs catalyst surface. In such a case, the scaling relation over  $\text{Co}_1\text{Ru}$  TCs in  $\text{NH}_3$  synthesis was decoupled. As such, the developed  $\text{Co}_1\text{Ru}$  TCs presented a much higher  $\text{NH}_3$  synthesis rate and lower reaction activation energy than those of  $\text{Co}_1\text{Ru}$  dual atoms (DAs) and  $\text{Co}_1\text{Ru}$  nanoparticles (NPs). Furthermore, Zhang *et al.* prepared a series of  $\text{M}_1\text{Ru}$  SAA catalysts by the anchoring of transition-metal single atom (Fe, Co, and Ni) onto Ru nanoclusters.<sup>106</sup> They found that  $\text{Co}_1\text{Ru}$  SAA has the highest  $\text{NH}_3$  synthesis rate and the largest  $\text{TOF}_{\text{Ru}}$  value among various  $\text{M}_1\text{Ru}$  SAA (Fig. 9a). Compared with the  $\text{CoRu}$  nanoparticle alloy (NPA), various characterizations elucidated that  $\text{Co}_1\text{Ru}$  SAA possessed stronger electronic interaction between Co and Ru, which induced lower work function and up-shift d band center toward the Fermi level, thus accelerating the activation of  $\text{N}_2$ . Meanwhile, the unique SAA structure could effectively tune the  $\text{N}_2$  activation pathway. DRIFTS technique showed that the  $^*\text{N}_2\text{D}_x$  intermediates can be observed over  $\text{Co}_1\text{Ru}$  SAA under the atmosphere of 25%  $\text{N}_2$ –75%  $\text{D}_2$ , demonstrating that  $\text{N}_2$  molecules can be activated *via* an associative mechanism, accounting for efficient  $\text{NH}_3$  synthesis at mild conditions (Fig. 9b).

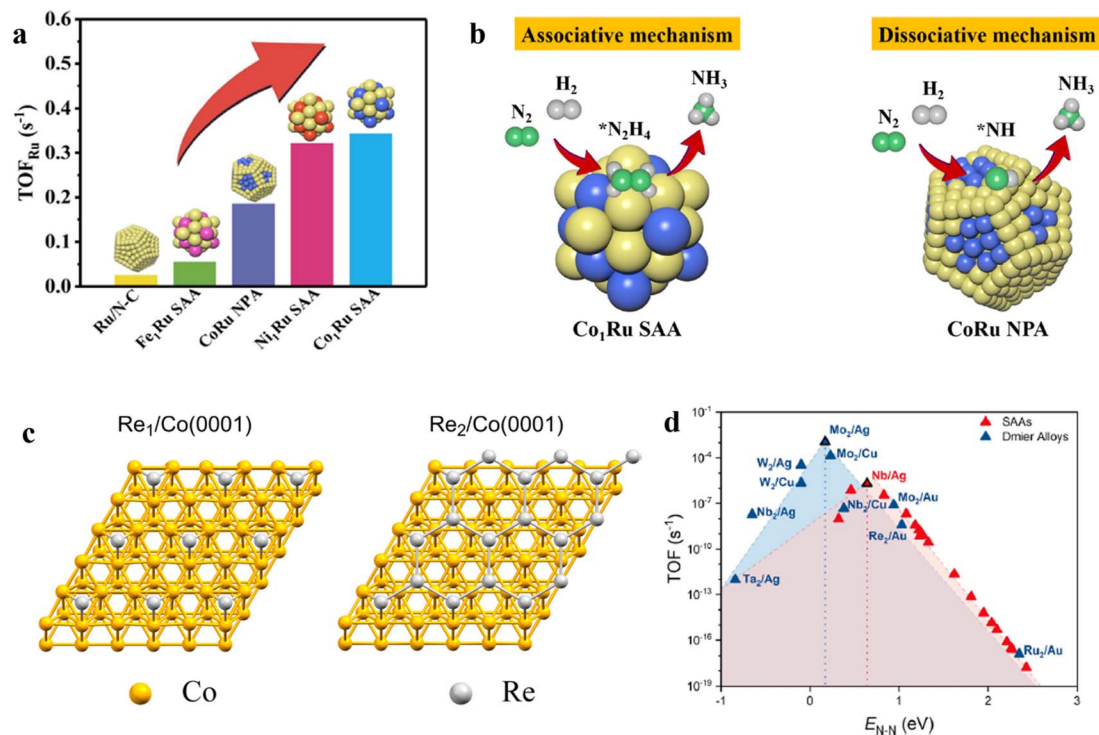


**Fig. 9** (a)  $\text{TOF}_{\text{Ru}}$  values over the as-synthesized catalysts at 400 °C and 1 MPa. (b) The proposed  $\text{N}_2$  activation pathway over  $\text{Co}_1\text{Ru}$  SAA and  $\text{CoRu}$  NPA.<sup>106</sup> (c) Top views of free  $\text{Re}_1$  and  $\text{Re}_2$  centers over  $\text{Co}(0001)$ .<sup>107</sup> (d) Comparison of the volcano plot of TOF for dimer alloys and SAAs as a function of  $^*\text{N-N}$  transition state energies.<sup>107</sup> The TOF is calculated at 673 K,  $P_{\text{N}_2} = 24.5$  bar,  $P_{\text{H}_2} = 74.25$  bar,  $P_{\text{NH}_3} = 1$  bar, and 2% conversion to  $\text{NH}_3$ . TOFs of  $\text{Mo}_2/\text{Au}$ ,  $\text{Ru}_2/\text{Au}$ , and  $\text{Re}_2/\text{Au}$  dimer alloys are calculated using the DFT results reported in ref. 109.



In addition, Cholach *et al.* investigated the active centers of one or a pair of Re atoms on the Co(0001) support for NH<sub>3</sub> synthesis using DFT calculation (Fig. 9c).<sup>107</sup> They found that the binding N to Re and Co can significantly reduce the heat of dissociative adsorption of N<sub>2</sub> in the cases of Re<sub>1</sub>/Co(0001), Re<sub>2</sub>/Co(0001), and Re(0001). As a result, the specific TOF on the basis of Re<sub>1</sub>/Co(0001), Re<sub>2</sub>/Co(0001), and the plane Re(0001) changed in the order of  $8.0 \times 10^3$ , 32.0, and 1.0, respectively. They also demonstrated that the Re single atom on the Co(0001) support exhibited a much higher NH<sub>3</sub> synthesis performance than that of Re dual atoms. Nevertheless, when the host metal was changed into either Cu(111) or Ag(111), the transition-metal single atom or dimer atoms supported on Ag(111) or Cu(111) catalysts presented different trends. Zhang *et al.* revealed that the Nb/Ag SAA was located at the volcano peak of NH<sub>3</sub> synthesis on the basis of the TM<sub>1</sub>/Ag(111) system, while the Mo<sub>2</sub>/Ag dimer alloy exhibited a much higher TOF value compared with Nb/Ag SAA (Fig. 9d).<sup>108</sup> DFT calculations showed that the Mo<sub>2</sub>/Ag dimer alloy has a lower N<sub>2</sub> activation energy and weaker N absorption than that of Nb/Ag SAA, *i.e.*, the BEP relationship for N<sub>2</sub> dissociation derived on dimer alloys is closer to the ideal limit in comparison to that obtained on SAAs, leading to the higher activities of dimer alloys for NH<sub>3</sub> synthesis.

Although M<sub>1</sub>Ru SAAs have been reported to exhibit considerable NH<sub>3</sub> synthesis performance experimentally, while this

kind of SAAs are based on the Ru as the host metal atoms in SAAs. The development of SAAs with single-atom Ru as the guest metal atom in SAAs for NH<sub>3</sub> synthesis is more appealing, especially for reducing the content of noble Ru metal. In addition, the predicted higher NH<sub>3</sub> synthesis performance of dimer alloys than SAAs provides a wide platform to exploit more efficient catalysts for NH<sub>3</sub> synthesis. Developing advanced methods for the preparation of dimer alloys is really worth exploring.

## 5. Conclusions and prospects

The development of efficient catalysts for NH<sub>3</sub> synthesis under mild conditions has been a long-term endeavor in this field. The remarkable differences in the geometric and electronic structure of active sites at different scales stimulate that the single-atom and cluster catalysts exhibit significantly distinct catalytic performance and reaction mechanism compared with nanoparticle catalysts. Based on the analysis in this review, the main differences between nanoparticle catalysts, single-atom and cluster catalysts are summarized by the following three aspects:

### 5.1 Hydrogen poisonous

Nanoparticle catalysts usually suffer from unavoidable hydrogen poisoning due to the strong adsorption of H species on the nanoparticle surface, while the hydrogen poisonous was

**Table 1** Catalytic properties for NH<sub>3</sub> synthesis over various SACs, SCCs, and BCCs catalysts

Catalyst		Metal content (wt%)	Reaction conditions			NH <sub>3</sub> synthesis rate (mmol <sub>NH<sub>3</sub></sub> g <sub>cat</sub> <sup>-1</sup> h <sup>-1</sup> )	Ref.
			Temperature (°C)	Pressure (MPa)	WHSV (mL g <sup>-1</sup> h <sup>-1</sup> )		
SACs	Co-N-C	3.8	350	1.0	60 000	4.34	48
	Ba-Ru SAs/S-1	0.27	400	0.1	18 000	1.39	63
	Ru/HZ SAC	0.2	300	1.0	60 000	2.52	65
	MoH <sub>x</sub>	2.0	400	0.1	12 000	0.026	72
	Co-N <sub>2</sub>	3.2	300	1.0	60 000	2.7	69
	FeN <sub>4</sub> @G-K	2.1	190	0.1	30 000	$10.3 \times 10^{-3}$	71
	Ru/CeO <sub>2</sub> (SAC)	1.00	450	1.0	72 000	9.9	119
	Ru SAC	0.39	400	1.0	60 000	4.7	49
	1.4 nm Ru NCs	1.18	400	1.0	60 000	17.1	19
	2.0 nm Ru NCs	1.06	400	1.0	60 000	8.8	19
SCCs	Ru <sub>3,0</sub> /BaCeO <sub>3</sub>	0.44	400	1.0	60 000	3.4	75
	Ru <sub>1,1</sub> /BaCeO <sub>3</sub>	0.46	400	1.0	60 000	19.4	75
	Ru/MgO-MIL	3.00	400	1.0	15 000	4.5	76
	Ru clusters/CeO <sub>2</sub>	5.00	400	1.0	—	28.0	79
	0.5Ru-SNCs	0.49	400	3.0	60 000	11.7	85
	Ru ACCs	0.40	400	1.0	60 000	7.4	49
	Ru-2.8 nm	0.44	400	1.0	60 000	2.9	49
	5% Ru/Sm <sub>2</sub> O <sub>3</sub> (activated)	5.00	400	1.0	24 000	32.2	82
	Ru/Sm <sub>2</sub> O <sub>3</sub>	5.00	400	1.0	24 000	23.0	81
	Co <sub>2</sub> ACCs	0.90	400	1.0	60 000	8.5	20
	Ba/Co <sub>2</sub> ACCs	0.90	400	1.0	60 000	19.4	20
	Co <sub>1</sub> Ru <sub>2</sub> /NC	1.17Ru + 0.41Co	400	3.0	60 000	18.9	95
	Ru-Co clusters@N-C	—	400	1.0	12 000	0.78	96
	Ru clusters@N-C	—	400	1.0	12 000	0.32	96
	Co <sub>1</sub> Ru SAA	1.05Ru + 0.30Co	400	1.0	60 000	4.38	105
BCCs	Fe <sub>1</sub> Ru SAA	1.36Ru + 0.47Fe	400	1.0	60 000	0.70	105
	Ni <sub>1</sub> Ru SAA	1.07Ru + 0.51Ni	400	1.0	60 000	2.90	105
	CoRu NPA	0.95Ru + 0.29Co	400	1.0	60 000	2.09	105



largely alleviated or eliminated on cluster catalysts.<sup>110–112</sup> The probable reasons may be attributed to that the emergence of discrete d and sp bands of cluster atoms can alter the adsorption strength of N<sub>2</sub> and H<sub>2</sub> molecules, avoiding hydrogen poisonous or the increased interface of the metal-support can promote the hydrogen spillover to support and thus eliminate hydrogen poisonous.<sup>49,75</sup>

## 5.2 Reaction mechanism

The dissociative mechanism is preferred to occur on nanoparticle catalysts because of the presence of multiple atomic sites, such as Ru B<sub>5</sub> sites or Fe C<sub>7</sub> sites, which are highly active for the dissociation of N<sub>2</sub> molecules.<sup>31,33</sup> In terms of single-atom and cluster catalysts, the associative mechanism is suggested to be dominant even though satisfactory evidence is still needed to support this opinion.

## 5.3 Catalytic performance

By comparing the performance of different-size catalysts (Table 1), the cluster catalysts exhibit higher NH<sub>3</sub> synthesis rates than nanoparticle catalysts and single-atom catalysts thanks to the exposure of more active sites and/or different reaction mechanisms.<sup>49,113</sup> Concerning single-atom catalysts, the NH<sub>3</sub> synthesis rates are generally low in spite of their high dispersion.<sup>113,114</sup> The underlying reason could be the difficulty of simultaneous activation of N<sub>2</sub> and H<sub>2</sub> reactants on a single-atom site. To be noted, Ru species exist as large nanoparticles (≥2 nm) in industrial Ru-based catalysts. The higher catalytic performance of Ru clusters than Ru particles makes it possible to reduce the Ru content of commercial catalysts in the form of stable Ru clusters.

It is worth noting that the exploitation of single-atom and cluster catalysts for NH<sub>3</sub> synthesis with high-efficiency has gained more and more attention. With the advancement of preparation method and characterization techniques, an increasing number of single-atom and cluster catalysts would be developed for NH<sub>3</sub> synthesis. In the future, some research fields in terms of single-atom and cluster catalysts are promising to further improve the catalyst performance and deepen the fundamental understanding of structure–activity relationship as well as the reaction mechanism for NH<sub>3</sub> synthesis.

Fabricating the uniform active sites in SCCs or BCCs is still a great challenge. In terms of performance for NH<sub>3</sub> synthesis, SCCs or BCCs are superior to SACs and nanoparticle catalysts. Nevertheless, the preparation of uniform and exclusive structural SCCs or BCCs is much more difficult than SACs and nanoparticle catalysts, and most researches on SCCs or BCCs were based on DFT calculations. Currently, the widely used synthesis methods for SCCs or BCCs are the control of low metal loading or high-temperature pyrolysis, which are the lack of the precise manipulation of the location of metal species. With the usage of organometallic complex precursors containing atomic clusters and the application of advanced methods and instruments, it provides the possibility to precisely control the configuration and location of atomic clusters. Meanwhile, the precise construction of cluster sites can not only maximize

metal utilization but also provide platforms to investigate the reaction mechanism.

To better characterize the structure of single-atom and cluster catalysts as well as to detect the reaction intermediate species, it is necessary to develop advanced characterization techniques. Nowadays, the reaction mechanisms *via* the associative or dissociative pathway of single-atom and cluster catalysts are still under debate. The intermediates for NH<sub>3</sub> synthesis, such as NH<sub>x</sub> and N<sub>2</sub>H<sub>x</sub> species, are mainly detected by the UV-vis spectrum, *in situ* DRIFTS, and NEXAFS spectra.<sup>85,115,116</sup> The main reason is due to that these techniques would be possible to detect only those long-lived intermediates, which can give rise to a detectable population under steady-state conditions. Meanwhile, it is also difficult to accurately distinguish the spatial distribution of intermediates over different active sites based on *in situ* DRIFTS and NEXAFS spectra. The development of advanced characterization techniques, such as near ambient pressure X-ray photoelectron spectroscopy (NAP-XPS), TOF-SIMS, and neutron scattering techniques, would shed light on the analysis of catalyst structure and reaction mechanism in NH<sub>3</sub> synthesis.

The industrial application of NH<sub>3</sub> synthesis *via* an associative mechanism still faces long-term challenges, mainly focusing on the accessibility and durability of catalysts. Specifically, the application of catalysts with highly dispersed active sites is trapped in the metal agglomeration, *i.e.*, the growth of metal size from subnanometer to nanometer in the long-period operation. As a result, the NH<sub>3</sub> synthesis mechanism is changed from associative route to dissociative route during the reaction process, possibly accompanied by the decrease in the NH<sub>3</sub> synthesis rate. Moreover, the large-scale preparation of single-atom and cluster catalysts in the industry is still tough because of the complicated synthetic method and the difficulty of controlling the homogeneous dispersion of low-loading metal. Therefore, more efforts are needed to solve the stability and large-scale preparation of advanced single-atom and cluster catalysts before industrial application.

Artificial intelligence (AI)-assisted catalyst design will accelerate the development of efficient single-atom and cluster catalysts for NH<sub>3</sub> synthesis.<sup>117,118</sup> Traditional catalysts were discovered through trial-and-error method coupled with chemical intuition. In the early days of NH<sub>3</sub> synthesis research, thousands of catalysts were prepared and tested to find a catalyst suitable for industrialization. Nowadays, we are still trying new types of catalysts in order to improve the NH<sub>3</sub> synthesis activity at lower temperatures and pressure conditions. With the assistance of artificial intelligence, especially for automatic machine-learning, it shows enormous potential to accelerate the predictive discovery of novel catalyst formulations. Meanwhile, the combination of machine-learning methodology and high-throughput experimentation can greatly shorten the period of discovery of efficient catalysts for NH<sub>3</sub> synthesis.

## Author contributions

Conceptualization, investigation and writing – original draft: X. Peng, M. Zhang and T. Zhang. Conceptualization and writing –





review and editing: Y. Zhou and X. Wang. Investigation: Jun Ni. Funding acquisition and writing – review and editing: X. Wang. Funding acquisition and supervision: L. Jiang.

## Conflicts of interest

The authors declare no conflict of interest.

## Acknowledgements

The work was supported by the National Natural Science Foundation of China (22222801, 2221005, 22038002, 92361303, 22108037), National Key Research and Development Program (2022YFA1604101, 2021YFB4000400).

## References

- 1 Z. W. Seh, J. Kibsgaard, C. F. Dickens, I. Chorkendorff, J. K. Nørskov and T. F. Jaramillo, Combining theory and experiment in electrocatalysis: insights into materials design, *Science*, 2017, **355**, eaad4998.
- 2 K. Mazloomi and C. Gomes, Hydrogen as an energy carrier: prospects and challenges, *Renewable Sustainable Energy Rev.*, 2012, **16**, 3024–3033.
- 3 Y. Kojima and M. Yamaguchi, Ammonia as a hydrogen energy carrier, *Int. J. Hydrogen Energy*, 2022, **47**, 22832–22839.
- 4 P. Wang, H. Xie, J. Guo, Z. Zhao, X. Kong, W. Gao, F. Chang, T. He, G. Wu and M. Chen, The formation of surface lithium–iron ternary hydride and its function on catalytic ammonia synthesis at low temperatures, *Angew. Chem., Int. Ed.*, 2017, **129**, 8842–8846.
- 5 T.-N. Ye, S.-W. Park, Y. Lu, J. Li, J. Wu, M. Sasase, M. Kitano and H. Hosono, Dissociative and associative concerted mechanism for ammonia synthesis over Co-based catalyst, *J. Am. Chem. Soc.*, 2021, **143**, 12857–12866.
- 6 C. Zamfirescu and I. Dincer, Using ammonia as a sustainable fuel, *J. Power Sources*, 2008, **185**, 459–465.
- 7 C. H. Christensen, T. Johannessen, R. Z. Sørensen and J. K. Nørskov, Towards an ammonia-mediated hydrogen economy, *Catal. Today*, 2006, **111**, 140–144.
- 8 N. Kuganathan, H. Hosono, A. L. Shluger and P. V. Sushko, Enhanced N<sub>2</sub> dissociation on Ru-loaded inorganic electride, *J. Am. Chem. Soc.*, 2014, **136**, 2216–2219.
- 9 H. Liu, Ammonia synthesis catalyst 100 years: practice, enlightenment and challenge, *Chin. J. Catal.*, 2014, **35**, 1619–1640.
- 10 K. Sato and K. Nagaoka, Boosting ammonia synthesis under mild reaction conditions by precise control of the basic oxide–Ru interface, *Chem. Lett.*, 2021, **50**, 687–696.
- 11 J. Wang, L. Yu, L. Hu, G. Chen, H. Xin and X. Feng, Ambient ammonia synthesis via palladium-catalyzed electrohydrogenation of dinitrogen at low overpotential, *Nat. Commun.*, 2018, **9**, 1795–1802.
- 12 T. Ogawa, Y. Kobayashi, H. Mizoguchi, M. Kitano, H. Abe, T. Tada, Y. Toda, Y. Niwa and H. Hosono, High electron density on Ru in intermetallic YRu<sub>2</sub>: the application to catalyst for ammonia synthesis, *J. Phys. Chem. C*, 2018, **122**, 10468–10475.
- 13 A. Vojvodic, A. J. Medford, F. Studt, F. Abild-Pedersen, T. S. Khan, T. Bligaard and J. Nørskov, Exploring the limits: a low-pressure, low-temperature Haber–Bosch process, *Chem. Phys. Lett.*, 2014, **598**, 108–112.
- 14 M. Kitano, Y. Inoue, Y. Yamazaki, F. Hayashi, S. Kanbara, S. Matsuishi, T. Yokoyama, S.-W. Kim, M. Hara and H. Hosono, Ammonia synthesis using a stable electride as an electron donor and reversible hydrogen store, *Nat. Chem.*, 2012, **4**, 934–940.
- 15 J. Qian, Q. An, A. Fortunelli, R. J. Nielsen and W. A. Goddard III, Reaction mechanism and kinetics for ammonia synthesis on the Fe (111) surface, *J. Am. Chem. Soc.*, 2018, **140**, 6288–6297.
- 16 J. W. Erisman, M. A. Sutton, J. Galloway, Z. Klimont and W. Winiwarter, How a century of ammonia synthesis changed the world, *Nat. Geosci.*, 2008, **1**, 636–639.
- 17 G. Xu, C. Cai and T. Wang, Toward Sabatier optimal for ammonia synthesis with paramagnetic phase of ferromagnetic transition metal catalysts, *J. Am. Chem. Soc.*, 2022, **144**, 23089–23095.
- 18 J. Wang, W. Cui, Q. Liu, Z. Xing, A. M. Asiri and X. Sun, Recent progress in cobalt-based heterogeneous catalysts for electrochemical water splitting, *Adv. Mater.*, 2016, **28**, 215–230.
- 19 X. Peng, X. Chen, Y. Zhou, F. Sun, T. Zhang, L. Zheng, L. Jiang and X. Wang, Size-dependent activity of supported Ru catalysts for ammonia synthesis at mild conditions, *J. Catal.*, 2022, **408**, 98–108.
- 20 X. Peng, H. Cai, Y. Zhou, J. Ni, X. Wang, B. Lin, J. Lin, L. Zheng, C.-t. Au and L. Jiang, Studies of a highly active cobalt atomic cluster catalyst for ammonia synthesis, *ACS Sustain. Chem. Eng.*, 2022, **10**, 1951–1960.
- 21 M. A. Shipman and M. D. Symes, Recent progress towards the electrosynthesis of ammonia from sustainable resources, *Catal. Today*, 2017, **286**, 57–68.
- 22 G. Ertl, Reactions at surfaces: from atoms to complexity (Nobel lecture), *Angew. Chem., Int. Ed.*, 2008, **47**, 3524–3535.
- 23 M. J. Bezdek and P. J. Chirik, Expanding boundaries: N<sub>2</sub> cleavage and functionalization beyond early transition metals, *Angew. Chem., Int. Ed.*, 2016, **55**, 7892–7896.
- 24 H.-P. Jia and E. A. Quadrelli, Mechanistic aspects of dinitrogen cleavage and hydrogenation to produce ammonia in catalysis and organometallic chemistry: relevance of metal hydride bonds and dihydrogen, *Chem. Soc. Rev.*, 2014, **43**, 547–564.
- 25 S. Zhang, Y. Zhao, R. Shi, G. I. Waterhouse and T. Zhang, Photocatalytic ammonia synthesis: recent progress and future, *EnergyChem*, 2019, **1**, 100013.
- 26 L. Ouyang, J. Liang, Y. Luo, D. Zheng, S. Sun, Q. Liu, M. S. Hamdy, X. Sun and B. Ying, Recent advances in electrocatalytic ammonia synthesis, *Chin. J. Catal.*, 2023, **50**, 6–44.
- 27 J. Zhao and Z. Chen, Single Mo atom supported on defective boron nitride monolayer as an efficient electrocatalyst for



- nitrogen fixation: a computational study, *J. Am. Chem. Soc.*, 2017, **139**, 12480–12487.
- 28 P. Emmett and S. Brunauer, The adsorption of nitrogen by iron synthetic ammonia catalysts, *J. Am. Chem. Soc.*, 1934, **56**, 35–41.
  - 29 G. Ertl, Surface science and catalysis-studies on the mechanism of ammonia synthesis: the PH Emmett award address, *Catal. Rev.: Sci. Eng.*, 1980, **21**, 201–223.
  - 30 G. Ertl, Elementary steps in heterogeneous catalysis, *Angew. Chem., Int. Ed.*, 1990, **29**, 1219–1227.
  - 31 D. R. Strongin, J. Carrazza, S. R. Bare and G. A. Somorjai, The importance of C<sub>7</sub> sites and surface roughness in the ammonia synthesis reaction over iron, *J. Catal.*, 1987, **103**, 213–215.
  - 32 K. Reuter, C. P. Plaisance, H. Oberhofer and M. Andersen, Perspective: on the active site model in computational catalyst screening, *J. Chem. Phys.*, 2017, **146**, 040901.
  - 33 K. Honkala, A. Hellman, I. Remediakis, A. Logadottir, A. Carlsson, S. Dahl, C. H. Christensen and J. K. Nørskov, Ammonia synthesis from first-principles calculations, *Science*, 2005, **307**, 555–558.
  - 34 N. Spencer, R. Schoonmaker and G. A. Somorjai, Iron single crystals as ammonia synthesis catalysts: effect of surface structure on catalyst activity, *J. Catal.*, 1982, **74**, 129–135.
  - 35 D. Strongin, S. Bare and G. A. Somorjai, The effects of aluminum oxide in restructuring iron single crystal surfaces for ammonia synthesis, *J. Catal.*, 1987, **103**, 289–301.
  - 36 D. Strongin and G. A. Somorjai, The effects of potassium on ammonia synthesis over iron single-crystal surfaces, *J. Catal.*, 1988, **109**, 51–60.
  - 37 G. A. Somorjai and N. Materer, Surface structures in ammonia synthesis, *Top. Catal.*, 1994, **1**, 215–231.
  - 38 J. J. Mortensen, L. B. Hansen, B. Hammer and J. K. Nørskov, Nitrogen adsorption and dissociation on Fe (111), *J. Catal.*, 1999, **182**, 479–488.
  - 39 S. Dahl, A. Logadottir, R. Egeberg, J. Larsen, I. Chorkendorff, E. Törnqvist and J. K. Nørskov, Role of steps in N<sub>2</sub> activation on Ru (0001), *Phys. Rev. Lett.*, 1999, **83**, 1814–1819.
  - 40 S. Dahl, E. Törnqvist and I. Chorkendorff, Dissociative adsorption of N<sub>2</sub> on Ru (0001): a surface reaction totally dominated by steps, *J. Catal.*, 2000, **192**, 381–390.
  - 41 S. Dahl, J. Sehested, C. Jacobsen, E. Törnqvist and I. Chorkendorff, Surface science based microkinetic analysis of ammonia synthesis over ruthenium catalysts, *J. Catal.*, 2000, **192**, 391–399.
  - 42 J. M. G. Carballo, J. Yang, A. Holmen, S. García-Rodríguez, S. Rojas, M. Ojeda and J. L. G. Fierro, Catalytic effects of ruthenium particle size on the Fischer–Tropsch synthesis, *J. Catal.*, 2011, **284**, 102–108.
  - 43 H. Fang, D. Liu, Y. Luo, Y. Zhou, S. Liang, X. Wang, B. Lin and L. Jiang, Challenges and opportunities of Ru-based catalysts toward the synthesis and utilization of ammonia, *ACS Catal.*, 2022, **12**, 3938–3954.
  - 44 P. Wang, F. Chang, W. Gao, J. Guo, G. Wu, T. He and P. Chen, Breaking scaling relations to achieve low-temperature ammonia synthesis through LiH-mediated nitrogen transfer and hydrogenation, *Nat. Chem.*, 2017, **9**, 64–70.
  - 45 Y. Gong, J. Wu, M. Kitano, J. Wang, T.-N. Ye, J. Li, Y. Kobayashi, K. Kishida, H. Abe, Y. Niwa, H. Yang, T. Tada and H. Hosono, Ternary intermetallic LaCoSi as a catalyst for N<sub>2</sub> activation, *Nat. Catal.*, 2018, **1**, 178–185.
  - 46 Y. Kobayashi, Y. Tang, T. Kageyama, H. Yamashita, N. Masuda, S. Hosokawa and H. Kageyama, Titanium-based hydrides as heterogeneous catalysts for ammonia synthesis, *J. Am. Chem. Soc.*, 2017, **139**, 18240–18246.
  - 47 J.-C. Liu, X.-L. Ma, Y. Li, Y.-G. Wang, H. Xiao and J. Li, Heterogeneous Fe<sub>3</sub> single-cluster catalyst for ammonia synthesis via an associative mechanism, *Nat. Commun.*, 2018, **9**, 1610–1619.
  - 48 X. Wang, X. Peng, W. Chen, G. Liu, A. Zheng, L. Zheng, J. Ni, C.-t. Au and L. Jiang, Insight into dynamic and steady-state active sites for nitrogen activation to ammonia by cobalt-based catalyst, *Nat. Commun.*, 2020, **11**, 653–663.
  - 49 L. Li, Y.-F. Jiang, T. Zhang, H. Cai, Y. Zhou, B. Lin, X. Lin, Y. Zheng, L. Zheng and X. Wang, Size sensitivity of supported Ru catalysts for ammonia synthesis: from nanoparticles to subnanometric clusters and atomic clusters, *Chem*, 2022, **8**, 749–768.
  - 50 J. Li, Y. Li and T. Zhang, Recent progresses in the research of single-atom catalysts, *Sci. China Mater.*, 2020, **63**, 889–891.
  - 51 E. C. Tyo and S. Vajda, Catalysis by clusters with precise numbers of atoms, *Nat. Nanotechnol.*, 2015, **10**, 577–588.
  - 52 Q. Yang, Y. Jiang, H. Zhuo, E. M. Mitchell and Q. Yu, Recent progress of metal single-atom catalysts for energy applications, *Nano Energy*, 2023, 108404.
  - 53 B. Qiao, A. Wang, X. Yang, L. F. Allard, Z. Jiang, Y. Cui, J. Liu, J. Li and T. Zhang, Single-atom catalysis of CO oxidation using Pt<sub>1</sub>/FeO<sub>x</sub>, *Nat. Chem.*, 2011, **3**, 634–641.
  - 54 Y. Zhou, F. Wei, H. Qi, Y. Chai, L. Cao, J. Lin, Q. Wan, X. Liu, Y. Xing and S. Lin, Peripheral-nitrogen effects on the Ru<sub>1</sub> centre for highly efficient propane dehydrogenation, *Nat. Catal.*, 2022, **5**, 1145–1156.
  - 55 Q. He, Y. Meng, H. Zhang, Y. Zhang, Q. Sun, T. Gan, H. Xiao, X. He and H. Ji, Amino-metalloporphyrin polymers derived Fe single atom catalysts for highly efficient oxygen reduction reaction, *Sci. China: Chem.*, 2020, **63**, 810–817.
  - 56 F. Chen, X. Jiang, L. Zhang, R. Lang and B. Qiao, Single-atom catalysis: bridging the homo- and heterogeneous catalysis, *Chin. J. Catal.*, 2018, **39**, 893–898.
  - 57 Y. Wang, L. Chen, Z. Mao, L. Peng, R. Xiang, X. Tang, J. Deng, Z. Wei and Q. Liao, Controlled synthesis of single cobalt atom catalysts via a facile one-pot pyrolysis for efficient oxygen reduction and hydrogen evolution reactions, *Sci. Bull.*, 2019, **64**, 1095–1102.
  - 58 J. Liu, H. Lu, D. W. Zhang and M. Nolan, Reactions of ruthenium cyclopentadienyl precursor in the metal precursor pulse of Ru atomic layer deposition, *J. Mater. Chem. C*, 2021, **9**, 2919–2932.
  - 59 A. Wang, J. Li and T. Zhang, Heterogeneous single-atom catalysis, *Nat. Rev. Chem*, 2018, **2**, 65–81.



- 60 F. Huang, Y. Deng, Y. Chen, X. Cai, M. Peng, Z. Jia, P. Ren, D. Xiao, X. Wen and N. Wang, Atomically dispersed Pd on nanodiamond/graphene hybrid for selective hydrogenation of acetylene, *J. Am. Chem. Soc.*, 2018, **140**, 13142–13146.
- 61 X. Cui, X. Dai, A.-E. Surkus, K. Junge, C. Kreyenschulte, G. Agostini, N. Rockstroh and M. Beller, Zinc single atoms on N-doped carbon: an efficient and stable catalyst for CO<sub>2</sub> fixation and conversion, *Chin. J. Catal.*, 2019, **40**, 1679–1685.
- 62 J. M. Thomas, Tens of thousands of atoms replaced by one, *Nature*, 2015, **525**, 325–326.
- 63 J.-Z. Qiu, J. Hu, J. Lan, L.-F. Wang, G. Fu, R. Xiao, B. Ge and J. Jiang, Pure siliceous zeolite-supported Ru single-atom active sites for ammonia synthesis, *Chem. Mater.*, 2019, **31**, 9413–9421.
- 64 Á. Logadóttir and J. K. Nørskov, Ammonia synthesis over a Ru (0001) surface studied by density functional calculations, *J. Catal.*, 2003, **220**, 273–279.
- 65 X. Wang, L. Li, Z. Fang, Y. Zhang, J. Ni, B. Lin, L. Zheng, C.-t. Au and L. Jiang, Atomically dispersed Ru catalyst for low-temperature nitrogen activation to ammonia *via* an associative mechanism, *ACS Catal.*, 2020, **10**, 9504–9514.
- 66 F. Rosowski, A. Hornung, O. Hinrichsen, D. Herein, M. Muhler and G. Ertl, Ruthenium catalysts for ammonia synthesis at high pressures: preparation, characterization, and power-law kinetics, *Appl. Catal., A*, 1997, **151**, 443–460.
- 67 X. Wang, X. Peng, H. Ran, B. Lin, J. Ni, J. Lin and L. Jiang, Influence of Ru substitution on the properties of LaCoO<sub>3</sub> catalysts for ammonia synthesis: XAFS and XPS studies, *Ind. Eng. Chem. Res.*, 2018, **57**, 17375–17383.
- 68 A. Han, B. Wang, A. Kumar, Y. Qin, J. Jin, X. Wang, C. Yang, B. Dong, Y. Jia and J. Liu, Recent advances for MOF-derived carbon-supported single-atom catalysts, *Small Methods*, 2019, **3**, 1800471–1800492.
- 69 Y. Zhou, C. Wang, X. Peng, T. Zhang, X. Wang, Y. Jiang, H. Qi, L. Zheng, J. Lin and L. Jiang, Boosting efficient ammonia synthesis over atomically dispersed Co-based catalyst *via* the modulation of geometric and electronic structures, *CCS Chem.*, 2022, **4**, 1758–1769.
- 70 X. Li, Y. Jiao, Y. Cui, C. Dai, P. Ren, C. Song and X. Ma, Synergistic catalysis of the synthesis of ammonia with Co-based catalysts and plasma: from nanoparticles to a single atom, *ACS Appl. Mater. Interfaces*, 2021, **13**, 52498–52507.
- 71 Z. Chen, Y. Ye, T. Peng, C. Wu, H. Li, X. Pan and X. Bao, Iron-single sites confined by graphene lattice for ammonia synthesis under mild conditions, *ACS Catal.*, 2023, **13**, 14385–14394.
- 72 L. M. Azofra, N. Morlanés, A. Poater, M. K. Samantaray, B. Vidjayacoumar, K. Albahily, L. Cavallo and J. M. Basset, Single-site molybdenum on solid support materials for catalytic hydrogenation of N<sub>2</sub>-into-NH<sub>3</sub>, *Angew. Chem., Int. Ed.*, 2018, **57**, 15812–15816.
- 73 B. Lin, Y. Wu, B. Fang, C. Li, J. Ni, X. Wang, J. Lin and L. Jiang, Ru surface density effect on ammonia synthesis activity and hydrogen poisoning of ceria-supported Ru catalysts, *Chin. J. Catal.*, 2021, **42**, 1712–1723.
- 74 C. J. H. Jacobsen, S. Dahl, P. L. Hansen, E. Törnqvist, L. Jensen, H. Topsøe, D. V. Prip, P. B. Møenshaug and I. Chorkendorff, Structure sensitivity of supported ruthenium catalysts for ammonia synthesis, *J. Mol. Catal. A: Chem.*, 2000, **163**, 19–26.
- 75 Y. Zhou, J. Wang, L. Liang, Q. Sai, J. Ni, C.-t. Au, X. Lin, X. Wang, Y. Zheng, L. Zheng and L. Jiang, Unraveling the size-dependent effect of Ru-based catalysts on ammonia synthesis at mild conditions, *J. Catal.*, 2021, **404**, 501–511.
- 76 J. Li, W. Wang, W. Chen, Q. Gong, J. Luo, R. Lin, H. Xin, H. Zhang, D. Wang, Q. Peng, W. Zhu, C. Chen and Y. Li, Sub-nm ruthenium cluster as an efficient and robust catalyst for decomposition and synthesis of ammonia: break the “size shackles”, *Nano Res.*, 2018, **11**, 4774–4785.
- 77 L. D. Marks, Experimental studies of small particle structures, *Rep. Prog. Phys.*, 1994, **57**, 603–649.
- 78 F. Tao, S. Dag, L.-W. Wang, Z. Liu, D. R. Butcher, H. Bluhm, M. Salmeron and G. A. Somorjai, Break-up of stepped platinum catalyst surfaces by high CO coverage, *Science*, 2010, **327**, 850–853.
- 79 J. Feng, L. Liu, X. Ju, M. Wang, X. Zhang, J. Wang and P. Chen, Sub-nanometer Ru clusters on ceria nanorods as efficient catalysts for ammonia synthesis under mild conditions, *ACS Sustain. Chem. Eng.*, 2022, **10**, 10181–10191.
- 80 S. Hirabayashi, M. Ichihashi and Y. Takeda, Optimization of ruthenium particle size and ceria support for enhanced activity of Ru/CeO<sub>2</sub> cluster catalysts in ammonia synthesis under mild conditions, *Catal. Lett.*, 2023, **154**, 487–493.
- 81 J. Wang, L. Liu, X. Zhang, J. Yu, X. Ju, J. Feng, J. Guo, T. He and P. Chen, Sub-nanometer Ru clusters on Sm<sub>2</sub>O<sub>3</sub> obtained from a room temperature ion adsorption method for ammonia synthesis, *Catal. Sci. Technol.*, 2022, **12**, 7501–7509.
- 82 X. Zhang, L. Liu, A. Wu, J. Zhu, R. Si, J. Guo, R. Chen, Q. Jiang, X. Ju and J. Feng, Synergizing surface hydride species and Ru clusters on Sm<sub>2</sub>O<sub>3</sub> for efficient ammonia synthesis, *ACS Catal.*, 2022, **12**, 2178–2190.
- 83 Y. Zhang, S. Li, C. Sun, X. Cao, X. Wang and J. Yao, Defective g-C<sub>3</sub>N<sub>4</sub> supported Ru<sub>3</sub> single-cluster catalyst for ammonia synthesis through parallel reaction pathways, *Nano Res.*, 2023, **16**, 3580–3587.
- 84 Q.-Y. Fan, J.-L. Liu, F.-Q. Gong, Y. Wang and J. Cheng, Structural dynamics of Ru clusters during nitrogen dissociation in ammonia synthesis, *Phys. Chem. Chem. Phys.*, 2022, **24**, 10820–10825.
- 85 Y. Zhou, Q. Sai, Z. Tan, C. Wang, X. Wang, B. Lin, J. Ni, J. Lin and L. Jiang, Highly efficient subnanometer Ru-based catalyst for ammonia synthesis *via* an associative mechanism, *Chin. J. Chem. Eng.*, 2022, **43**, 177–184.
- 86 S. E. Sivan, K. H. Kang, S. J. Han, O. Francis Ngome Okello, S.-Y. Choi, V. Sudheeshkumar, R. W. J. Scott, H.-J. Chae, S. Park and U. H. Lee, Facile MOF-derived one-pot synthetic approach toward Ru single atoms, nanoclusters, and nanoparticles dispersed on CeO<sub>2</sub> supports for enhanced ammonia synthesis, *J. Catal.*, 2022, **408**, 316–328.





- 87 T. Bligaard, J. K. Nørskov, S. Dahl, J. Matthiesen, C. H. Christensen and J. Sehested, The Brønsted–Evans–Polanyi relation and the volcano curve in heterogeneous catalysis, *J. Catal.*, 2004, **224**, 206–217.
- 88 S. Dahl, A. Logadottir, C. J. H. Jacobsen and J. K. Nørskov, Electronic factors in catalysis: the volcano curve and the effect of promotion in catalytic ammonia synthesis, *Appl. Catal.*, A, 2001, **222**, 19–29.
- 89 A. J. Medford, A. Vojvodic, J. S. Hummelshøj, J. Voss, F. Abild-Pedersen, F. Studt, T. Bligaard, A. Nilsson and J. K. Nørskov, From the Sabatier principle to a predictive theory of transition-metal heterogeneous catalysis, *J. Catal.*, 2015, **328**, 36–42.
- 90 C. Cui, H. Zhang, R. Cheng, B. Huang and Z. Luo, On the nature of three-atom metal cluster catalysis for N<sub>2</sub> reduction to ammonia, *ACS Catal.*, 2022, **12**, 14964–14975.
- 91 L. Liu, M. Lopez-Haro, C. W. Lopes, S. Rojas-Buzo, P. Concepcion, R. Manzorro, L. Simonelli, A. Sattler, P. Serna, J. J. Calvino and A. Corma, Structural modulation and direct measurement of subnanometric bimetallic PtSn clusters confined in zeolites, *Nat. Catal.*, 2020, **3**, 628–638.
- 92 X. Li, Y. Zhou, B. Qiao, X. Pan, C. Wang, L. Cao, L. Li, J. Lin and X. Wang, Enhanced stability of Pt/Al<sub>2</sub>O<sub>3</sub> modified by Zn promoter for catalytic dehydrogenation of ethane, *J. Energy Chem.*, 2020, **51**, 14–20.
- 93 T. N. Ye, S. W. Park, Y. Lu, J. Li, M. Sasase, M. Kitano, T. Tada and H. Hosono, Vacancy-enabled N<sub>2</sub> activation for ammonia synthesis on an Ni-loaded catalyst, *Nature*, 2020, **583**, 391–395.
- 94 T. N. Ye, S. W. Park, Y. Lu, J. Li, J. Wu, M. Sasase, M. Kitano and H. Hosono, Dissociative and associative concerted mechanism for ammonia synthesis over Co-based catalyst, *J. Am. Chem. Soc.*, 2021, **143**, 12857–12866.
- 95 L. Nguyen, S. Zhang, L. Wang, Y. Li, H. Yoshida, A. Patlolla, S. Takeda, A. I. Frenkel and F. Tao, Reduction of nitric oxide with hydrogen on catalysts of singly dispersed bimetallic sites Pt<sub>1</sub>Co<sub>m</sub> and Pd<sub>1</sub>Co<sub>n</sub>, *ACS Catal.*, 2016, **6**, 840–850.
- 96 J. Ni, Z. Tan, Q. Sai, J. Zhu, X. Wang, B. Lin, J. Lin, C.-t. Au and L. Jiang, Target-oriented confinement of Ru-Co nanoparticles inside N-doped carbon spheres *via* a benzoic acid guided process for high-efficient low-temperature ammonia synthesis, *J. Energy Chem.*, 2021, **57**, 140–146.
- 97 J. Yang, D. He, W. Chen, W. Zhu, H. Zhang, S. Ren, X. Wang, Q. Yang, Y. Wu and Y. Li, Bimetallic Ru–Co clusters derived from a confined alloying process within zeolite–imidazolate frameworks for efficient NH<sub>3</sub> decomposition and synthesis, *ACS Appl. Mater. Interfaces*, 2017, **9**, 39450–39455.
- 98 S. Zhang, L. Nguyen, J. X. Liang, J. Shan, J. J. Liu, A. I. Frenkel, A. Patlolla, W. Huang, J. Li and F. F. Tao, Catalysis on singly dispersed bimetallic sites, *Nat. Commun.*, 2015, **6**, 7938.
- 99 X.-L. Ma, Y. Yang, L.-M. Xu, H. Xiao, W.-Z. Yao and J. Li, Theoretical investigation on hydrogenation of dinitrogen triggered by singly dispersed bimetallic sites, *J. Mater. Chem. A*, 2022, **10**, 6146–6152.
- 100 X. L. Ma, J. C. Liu, H. Xiao and J. Li, Surface single-cluster catalyst for N<sub>2</sub>-to-NH<sub>3</sub> thermal conversion, *J. Am. Chem. Soc.*, 2018, **140**, 46–49.
- 101 T. Nakao, T. Tada and H. Hosono, Transition metal-doped Ru nanoparticles loaded on metal hydrides for efficient ammonia synthesis from first principles, *J. Phys. Chem. C*, 2020, **124**, 1529–1534.
- 102 R. Cheng, C. Cui and Z. Luo, Catalysis of dinitrogen activation and reduction by a single Fe<sub>13</sub> cluster and its doped systems, *Phys. Chem. Chem. Phys.*, 2023, **25**, 1196–1204.
- 103 R. T. Hannagan, G. Giannakakis, M. Flytzani-Stephanopoulos and E. C. H. Sykes, Single-atom alloy catalysis, *Chem. Rev.*, 2020, **120**, 12044–12088.
- 104 T. J. Zhang, A. G. Walsh, J. H. Yu and P. Zhang, Single-atom alloy catalysts: structural analysis, electronic properties and catalytic activities, *Chem. Soc. Rev.*, 2021, **50**, 569–588.
- 105 Y. Zhang, J. Li, J. Cai, L. Yang, T. Zhang, J. Lin, X. Wang, C. Chen, L. Zheng, C.-t. Au, B. Yang and L. Jiang, Construction of spatial effect from atomically dispersed Co anchoring on subnanometer Ru cluster for enhanced N<sub>2</sub>-to-NH<sub>3</sub> conversion, *ACS Catal.*, 2021, **11**, 4430–4440.
- 106 Y. Zhang, X. Peng, J. Deng, F. Sun, J. Cai, Y. Zhou, J. Ni, B. Lin, L. Zheng, X. Wang, J. Lin and L. Jiang, Tuning N<sub>2</sub> activation pathway over Ru/Co sub-nanometer alloy for efficient ammonia synthesis, *J. Catal.*, 2021, **404**, 440–450.
- 107 A. R. Cholach and A. A. Bryliakova, Re-Co alloys and single-atom Re catalysts in ammonia synthesis: a DFT study, *Mol. Catal.*, 2021, **513**, 111801.
- 108 Y. Zhang, S. Li, C. Sun, P. Wang, Y. Yang, D. Yi, X. Wang and J. Yao, Understanding and modifying the scaling relations for ammonia synthesis on dilute metal alloys: from single-atom alloys to dimer alloys, *ACS Catal.*, 2022, **12**, 9201–9212.
- 109 A. R. Singh, J. H. Montoya, B. A. Rohr, C. Tsai, A. Vojvodic and J. K. Nørskov, Computational design of active site structures with improved transition-state scaling for ammonia synthesis, *ACS Catal.*, 2018, **8**, 4017–4024.
- 110 M. Kitano, Y. Inoue, H. Ishikawa, K. Yamagata, T. Nakao, T. Tada, S. Matsuishi, T. Yokoyama, M. Hara and H. Hosono, Essential role of hydride ion in ruthenium-based ammonia synthesis catalysts, *Chem. Sci.*, 2016, **7**, 4036–4043.
- 111 Y. Zhou, C. Wang, X. Peng, T. Zhang, X. Wang, Y. Jiang, H. Qi, L. Zheng, J. Lin and L. Jiang, Boosting efficient ammonia synthesis over atomically dispersed Co-based catalyst *via* the modulation of geometric and electronic structures, *CCS Chem.*, 2022, **4**, 1758–1769.
- 112 S. Wu, Y.-K. Peng, T.-Y. Chen, J. Mo, A. Large, I. McPherson, H.-L. Chou, I. Wilkinson, F. Venturini, D. Grinter, P. Ferrer Escorihuela, G. Held and S. C. E. Tsang, Removal of hydrogen poisoning by electrostatically polar MgO support for low-pressure NH<sub>3</sub> synthesis at a high rate over the Ru catalyst, *ACS Catal.*, 2020, **10**, 5614–5622.
- 113 L. M. Azofra, N. Morlanes, A. Poater, M. K. Samantaray, B. Vidjayacoumar, K. Albahily, L. Cavallo and J. M. Basset, Single-site molybdenum on solid support materials for



- catalytic hydrogenation of  $N_2$ -into- $NH_3$ , *Angew. Chem., Int. Ed.*, 2018, **57**, 15812–15816.
- 114 J. Z. Qiu, J. B. Hu, J. G. Lan, L. F. Wang, G. Y. Fu, R. J. Xiao, B. H. Ge and J. X. Jiang, Pure siliceous zeolite-supported Ru single-atom active sites for ammonia synthesis, *Chem. Mater.*, 2019, **31**, 9413–9421.
- 115 H. Duan, J.-C. Liu, M. Xu, Y. Zhao, X.-L. Ma, J. Dong, X. Zheng, J. Zheng, C. S. Allen, M. Danaie, Y.-K. Peng, T. Issariyakul, D. Chen, A. I. Kirkland, J.-C. Buffet, J. Li, S. C. E. Tsang and D. O'Hare, Molecular nitrogen promotes catalytic hydrodeoxygenation, *Nat. Catal.*, 2019, **2**, 1078–1087.
- 116 Y. Zhou, C.-Q. Xu, Z. Tan, H. Cai, X. Wang, J. Li, L. Zheng, C.-t. Au, J. Li and L. Jiang, Integrating dissociative and associative routes for efficient ammonia synthesis over a TiCN-promoted Ru-based catalyst, *ACS Catal.*, 2022, **12**, 2651–2660.
- 117 L. H. Mou, T. T. Han, P. E. S. Smith, E. Sharman and J. Jiang, Machine learning descriptors for data-driven catalysis study, *Adv. Sci.*, 2023, **10**, 2301020.
- 118 T. Toyao, Z. Maeno, S. Takakusagi, T. Kamachi, I. Takigawa and K. Shimizu, Machine learning for catalysis informatics: recent applications and prospects, *ACS Catal.*, 2020, **10**, 2260–2297.
- 119 X.-C. Hu, X.-P. Fu, W.-W. Wang, X. Wang, K. Wu, R. Si, C. Ma, C.-J. Jia and C.-H. Yan, Ceria-supported ruthenium clusters transforming from isolated single atoms for hydrogen production *via* decomposition of ammonia, *Appl. Catal., B*, 2020, **268**, 118424–118437.

